Chapter 1 Introduction

1.1 Overview

Organic materials are widely used in daily life, such as in containers, clothes, and furniture, owing to various functions, low fabrication cost, and high practicability. Most commercially produced polymers are used as electrical insulators. However in 1963, Australians DE Weiss and coworkers reported one high conductivity polyacetylene derivative and achieved a fairly low resistance of 1.0 ohm/cm.[1-3] After studying in this field for many years, A. J. Heeger, H. Shirakawa, and A. G. MacDiarmid were honored by being awarded the Nobel Prize in chemistry (2000) for their discovery and development of conductive polymers.

Recently, many electronic devices have been fabricated using conductive polymers, such as organic thin film transistors (OTFTs),[4, 5] organic light-emitting diodes (OLEDs),[6, 7] and organic photovoltaic devices (OPVs).[8, 9] The advantages of organic electronic devices are based on their robustness, flexibility, portability, low cost, and simple fabrication process. This dissertation will focus on the fabrication of polymer light-emitting diodes (PLEDs) and organic photovoltaic (OPV) devices and the enhancement of their performances using a self-assembled microlens array (MLA).

1.2 Fabrication of a microlens array (MLA)

Microlens arrays are extensively used in optical-electronic systems due to their functions of collection, expansion, deflection, and reflection of light. In traditional optical applications, the optical elements are usually very large (ranging from about one centimeter to several meters) and heavy (ranging from about hundred grams to hundred kilograms). The fabrication of traditional optical elements mainly involves cutting, grinding and polishing; which is time and cost consumption. However, since the rapid development of micro-fabrication technologies in 1960s, the size of microelectronic devices has become smaller than ever and this has allowed the development of micro-optic applications. Recently, microlens or

microlens array has been applied to micro-electronic products, such as imager sensors (CCD or CMOS), image recorders (DSC), fiber transceiver modules, micro-electro-mechanic systems (MEMS), light-emitting diodes (LED), and flat panel displays (FPD). The fabrication technologies of MLA include photoresist (PR) reflowing and etch-transferring, direct laser-writing, laser ablating, and grey-scale mask lithographing etc. These methods are described following.

1.2.1 Photoresist (PR) reflow and etch-transfer [10]

The fabrication process involves PR-reflowing and etch-transferring as shown in Figure 1.1. The first step is to coat a layer of PR on a glass substrate. Then, the PR layer is exposed to illumination (G line, I line, or broad band in wavelength of the light sources) and is protected with the use of a mask. After the PR is developed, the protected area is preserved and the exposed area is eliminated. Finally, the PR is melted and becomes a convex-plane lens due to the effect of surface tension. However, the applications of a PR-lens are limited because most of the PR is discolored. In order to avoid discoloration of the PR-lens, the lens is usually transferred to the substrate using a dry-etching process such as reactive ion etching (RIE).

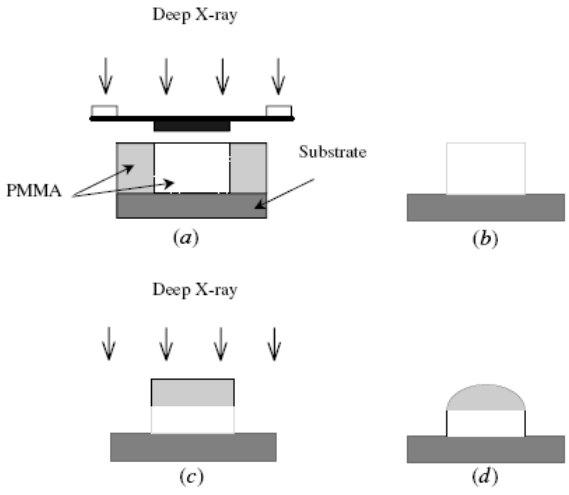

Figure 1.1 Fabrication processes of MLA (a) PR-coating and light-exposing, (b) developing, (c) re-exposing, and (d) thermal reflowing.[10]

1.2.2 Direct laser-writing [11]

Commercial laser lithographic systems are available for the fabrication of masks for use in semiconductor lithography. A non-continuous relief PR binary microstructure is fabricated using this method to function as a protective layer for the etching process. In contrast, a continuous PR structure is obtained using a direct laser-writing system to control the energy of laser. After absorbing the laser energy, the bonding of PR molecules is broken and then is able to be removed by developing. As a result, there is a relationship between the dose of laser beam and the corresponding relief height of PR film after development. After that, PR relief is transferred using electroforming and replicated using hot embossing.

1.2.3 Laser ablation [12]

In this method, an excimer laser (ArF 248nm and KrF 193nm in wavelength) is used to ablate material from the surface of substances such as polymers and glasses. Energy levels for the ablation of polymer materials are relatively low, typically from 0.1 to 1 J/cm^2. A continuous relief structure is obtained by varying the pulse repetition rates during the scan or by using a multiple scanning technique. The effective resolution capability of a current laser ablation system is above 1μm and is limited by the size of the ablated spots. The relief heights of the microstructures depend on the energy absorbed by the substrates. For the fabrication of a microlens array, a photomask with a special aperture is used to drag on the substrate surface in orthogonal directions. The fabrication process is simpler than the direct laser-writing method, which needs spin-coating, developing, and etch-transferring. However, the relief surface of fabricated microstructures using laser ablation is rough due to the discontinuous nature of the power density in a pulsed laser system.

1.2.4 Grey-scale mask lithography (Half-tone mask)

The height of a microstructure relief is determined by the repeat rate of the laser pulses and laser-beam shapes through a photomask when using the laser ablation method. In contrast,

the grey-scale lithographic method uses a continuous-wave light-source and the power density is determined by the aperture density or area-ratio. The advantage of the grey-scale lithographic method is that it can fabricate relief microstructures without photomask alignments and multiple lithographic processes. However, it is very difficult to realize well-defined curved edges on a microstructure using this method.

1.3 Organic light-emitting diodes (OLED)

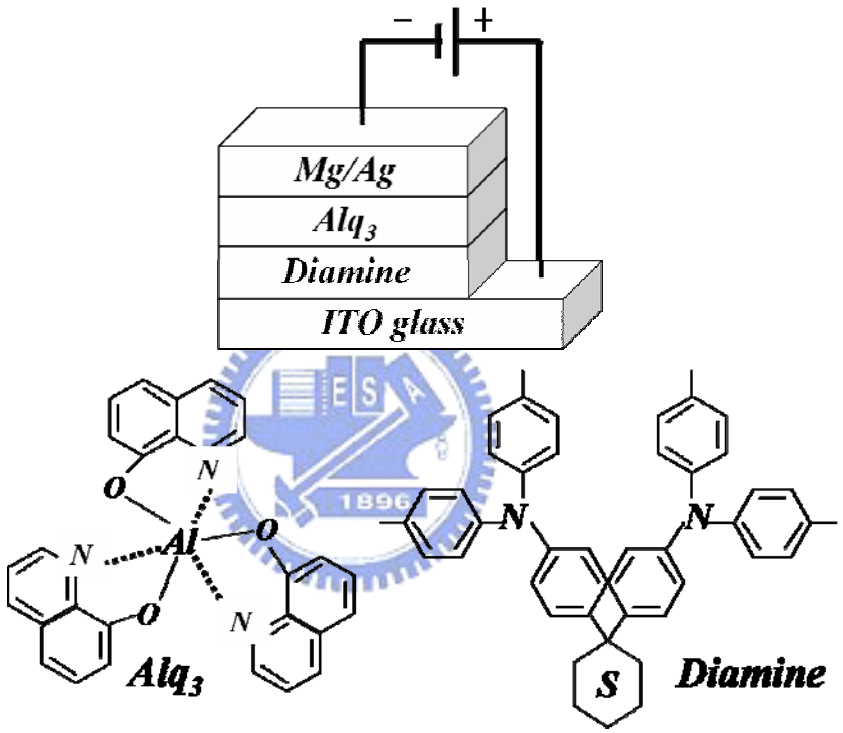

Figure 1.2 Device structure and organic materials in the OLED demonstrated by Tang and Vanslyke in 1987.

In 1953, Bernanose and coworkers first produced electroluminescence in organic materials by applying a high-voltage alternating current (AC) field to crystalline thin films of acridine orange and quinacrine.[13, 14] However, the operating voltage of the device was too high (>100V) to be suitable for industrial applications. It was not until 1987 that the next significant development took place: Tang and Van Slyke at Eastman Kodak demonstrated a high efficiency small-molecule OLED.[15] The OLED was composed of a derivative of

phenyl diamine as the hole-transporting layer and 8-hydroxyquinoline aluminum (Alq3) as both the electron-transporting and light-emitting layers as shown in Figure 1.2. High external quantum efficiency (1%), luminance efficiency (1.5lm/W), and brightness (>1000cd/m^2) were achieved at a driving voltage of less than 10V. At the Las Vegas CES 2007 Summit Sony showcased their 11 inch (28 cm, resolution 1,024 x 600) and 27 inch (68.5 cm, full HD resolution at 1920 x 1080) models which they claim have a million-to-one contrast ratio and a total thickness (including bezels) of 5 mm (Figure 1.3). However, the application of OLEDs over a large area is difficult because its organic thin-films have to be thermally evaporated under high vacuum conditions. As a response to this limitation, PLEDs were developed by Cambridge Display Technology (CDT) in 1990.{Rauscher, 1990 #85} The major advantage of PLEDs are that they involve a simpler fabricating process, such as spin-coating or ink-jet printing, which, in contrast to OLEDs, is suitable for application over large areas.

Figure 1.3: At the CES 2007, Sony displayed a pair of large-format widescreen OLED panels which are developed for future use in televisions.

OLEDs have attracted much attention due to their applications in flat panel displays (FPD). The advantages of an OLED include active emission, high contrast-ratio, wide viewing-angles, low power-consumption, low fabrication cost and light weight. OLEDs also have great potential to become flexible displays when they are fabricated on plastic substrates (PC, PET,

and PES etc.) and are suitable for large-area applications if a roll-to-roll process is used. However, there are still some challenges to be met before OLED becomes a commercial product. First, the organic materials of OLEDs are sensitive to humidity and oxygen; therefore, the packaging of devices should be improved to keep the concentration of water and oxygen at a minimum level of 1ppm/m^2/day. Second, the lifetime of OLED must exceed 100,000 hours for all red, green, and blue colors to fit the requirement of display applications. Third, large-area applications and mass-production are still problems.

1.3.1 Device structure of PLEDs

The device structure of PLEDs is composed of several sequenced layers: glass substrate, anode (indium tin oxide, ITO), hole transporting layer (HTL), light-emitting layer, and cathode (Ca/ Al or Mg/ Ag). Furthermore, a typical PLED is composed of a conjugated polymer such as poly[2-(2-ethylhexyloxy)-5-methoxy-1,4-phenylene vinylene], MEH-PPV or polyfluorene (PF) sandwiched between a transparent anode and a metal cathode on a glass or plastic substrate, as shown in Figure 1.4. Indium tin oxide is commonly used as the anode material. It is transparent and has a high work function which promotes the injection of holes into the polymer layer. By contrast, metals such as aluminium and calcium are often used for the cathode as they have low work functions which promote the injection of electrons into the polymer layer. Poly(3,4-ethylenedioxythiophene): poly(4-styrene sulfonate), or PEDOT:PSS as it is commonly referred to, is used to reduce the surface roughness of the anode and to improve the hole-injection efficiency between the anode and the organic layer. Under forward bias, positive carriers (holes) from the anode are injected into the HTL and the negative carriers (electrons) from the cathode are injected into the light-emitting layer. These positive and negative carriers recombine in the active layer and become excitons at excited states. After the excitons go to ground states, photons are generated as so-called electro-luminescence.

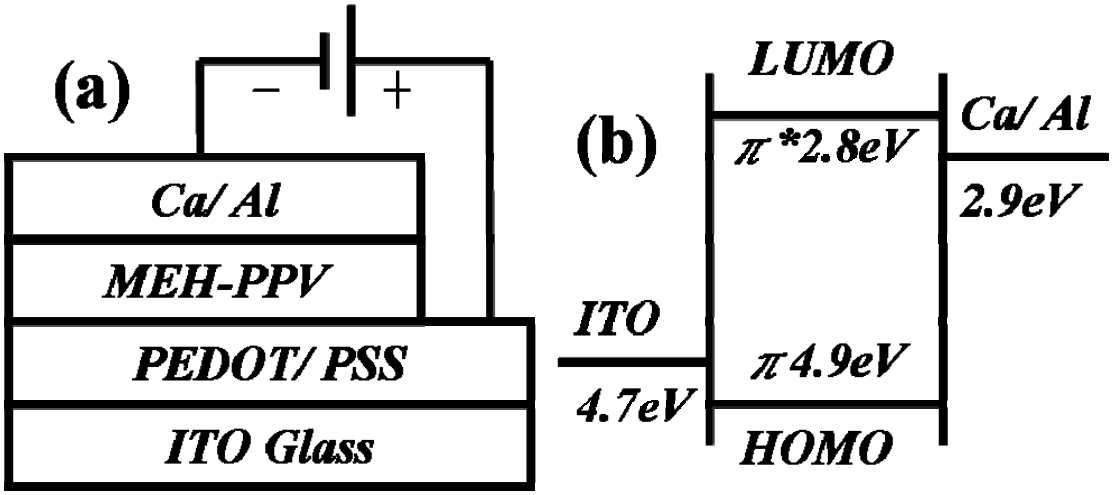

Figrue 1.4: (a) Device structure of a typical PLED with MEH-PPV as an active layer. (b) Band diagram of MEH-PPV and work functions of cathode and anode.

1.3.2 External quantum efficiency (EQE) of OLEDs

The EQE of an OLED is defined as the proportion of photons emitted outside the device in relation to the electron-hole pairs injected into the photoactive layer. The EQE can be represented as the following formula:

$$EQE = \eta_{cp}\eta_{\text{int}} = \gamma\eta_r\phi_f\eta_{cp}$$

where η_{int} is the internal quantum efficiency, η_{cp} is the light out-coupling efficiency, γ is the charge carriers balance factor (electron/ hole), η_r is the luminance efficiency of the excitons, and φ_f is the internal quantum efficiency of luminescence. Further, η_{int} is defined as a ratio of photons generated within the device in relation to the carriers injected into the active layer. Next, γ is the recombination ratio of the electrons and holes that are injected into the active layer. However, γ is smaller than one if the carriers pass through the active layer without recombination. In short, excitons are generated due to the recombination of electron-hole pairs and are excited by electric power. Two kinds of excitons are generated depending on the spin direction of the electrons. One kind, the singlet, has two electrons which spin in opposite orientations (S=0); in contrast, the triplet which is the other kind, has two parallel spinning electrons(S=1). A singlet emits light when it transits from the excited states to the ground

states; this emission is called fluorescence. In contrast, the light-emission of a triplet, which is called phosphorescence, is usually very weak since this process is spin forbidden. In a phosphorescence OLED, singlets formed on the host are transferred to the dopants by Förster energy transfer. Singlets undergo an intersystem cross (ISC) to triplets on the dopants with high efficiency due to their strong spin-orbital coupling. Triplets transfer energy directly to the dopants by Dexter energy transfer when they are created on the host. As a result, all singlet and triplet excitons contribute to the electroluminescence and this in turn results in η_r being close to 100%. Finally, η_{cp} is directly relative to the refractive indices of the materials used, the device structure, and the surface-shape of the substrate. However, η_{cp} is quite low due to the total internal reflections (TIR) and wave-guiding effects; in other words, most of the light generated in the active layer is trapped in the multi-layer structure. The proposed method to enhance η_{cp} is discussed in the following section

1.3.3 Enhanced light out-coupling efficiency of OLEDs

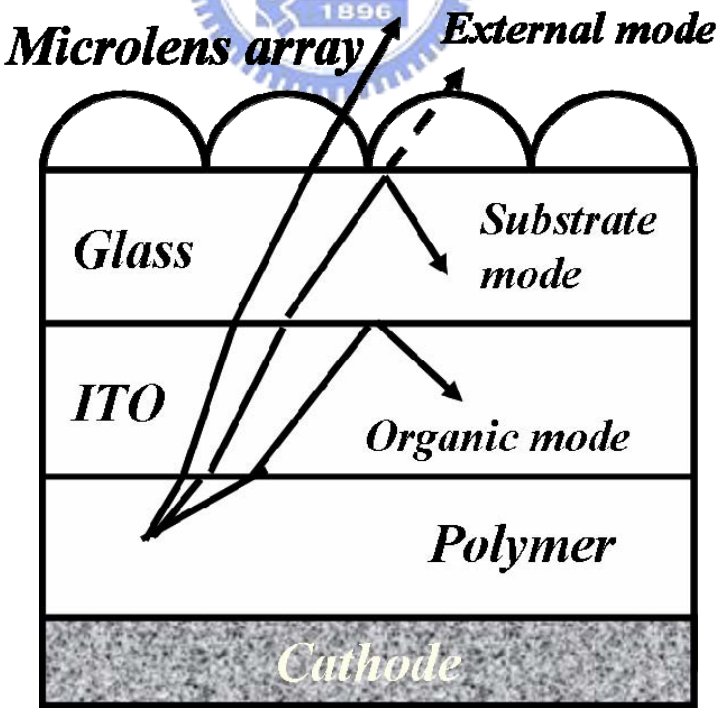

Figure 1.5 Device structure of PLED incorporated with a microlens array. Also shows the three radiation mode: external mode, substrate mode, and organic mode.

The generated light of OLEDs can be classified into three modes as shown in Figure 1.5. The external mode is the one escape from the device. The substrate mode is the light trapped in the glass substrate by the TIR at the air/glass interface. The organic mode is the light trapped by the TIR at the ITO/glass interface. Due to the mismatch of reflective-index between the emitting layer and the air, a large fraction of light is trapped in the glass substrate, ITO, and organic layers. Therefore, microlens or microlens array are used to enhance the η_p because the wave-guided modes have opportunities to become external modes due to the relief surfaces. Sturm *et al*. demonstrated a 2.3 fold enhancement using a hemisphere microlens where the OLED was placed at the center of the lens.[16, 17] Alternatively, Forrest *et al*. used a microlens array, which was replicated using a silicon mold, to get a 50% increase in η_{cp}.[18] However, the fore-mentioned methods use either a complicated process or result in color differences and field distortions. In this study, a simple fabrication method of OLEDs is proposed by incorporating of a self-assembled microlens array to enhance the η_{cp} without inducing any apparent color difference.

1.4 Organic photovoltaic (OPV) devices

Organic photovoltaic devices (OPV) which consist of conjugated polymer as electron donors (D) and fullerene derivatives as electron acceptors (A) have attracted much interest due to their simple fabrication process, high throughput, high flexibility, low weight, and low fabrication cost. Figure 1.6 shows the structure of a bulk-heterojunction (BHJ) OPV device, which is composed of an organic active layer, sandwiched between a transparent anode and a metal cathode. The materials used in the active layer are poly(3-hexylthiophene) (P3HT, MW=37680, PDI=1.48, purchased from Rieke Metals) as an electron donor and 6,6-phenyl C61-butyric acid methyl ester (PCBM, MW=9109, purchased from Uni-Region Bio-Tech) as an electron accepter. A modification layer, poly(3,4-ethylenedioxythiophene): poly(4-styrene sulfonate) (PEDOT:PSS), is used to improve hole-injection ability at the interface between the anode (ITO) and the active layer.

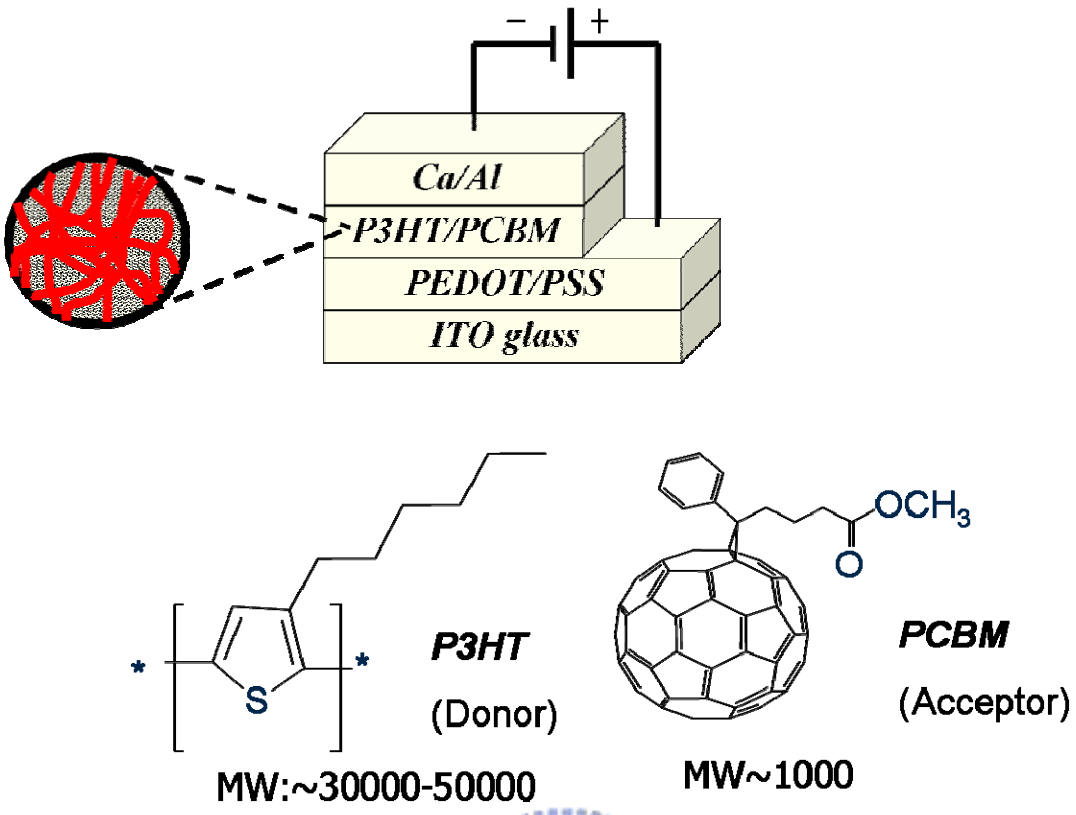

Figure 1.6 The OPV device is composes of ITO 100nm/ PEDOT: PSS 60nm/ P3HT: PCBM 200nm/ Ca 30nm/ Al 100nm. It also shows the donor material (P3HT) and the accepter material (PCBM) used in the OPV device.

Figure 1.7 shows, in sequence, the photocurrent generation mechanism in OPV devices which includes (1) light absorption, (2) exciton generation, (3) exciton diffusion, (4) electron-hole separation (exciton dissociation), (5) charge-carries transportation, and (6) charge-carriers collection. The donor material absorbs the incident light and generates excitons due to the photo-excited electrons being transferred from the π-HOMO to π*-LUMO bands. The light-absorption efficiency (η_A) is determined by the wavelength dependence absorption coefficient and the film-thickness of the donor. The donor material has a low ionization potential (IP) given by its highest occupied molecular orbital (HOMO) level, while the acceptor material has a high electron affinity (EA) given by its lowest unoccupied molecular orbital (LUMO) level. The exciton in the donor material has energy *E*ex which is

smaller than the energy gap between the LUMO and HOMO of the donor (*E*gap), by the exciton binding energy (typically between 0.1 and 0.2 eV in organics). During the exciton diffusion, Förster (long range) transfer or Dexter (between adjacent molecular) transfer takes place between the excited molecules and the molecules that receives the excitation. After the exciton diffuses to the D/A interface, it dissociates into the free electron and hole under the condition $E_{ex} > IP - EA$. Then, the electron and hole are transported in the accepter and donor materials, respectively. The charge-carriers transportation efficiency (η_T ~1) is determined by traps and the mobility of thin film. Finally, the generated charge-carriers are collected by the cathode and anode as the photocurrent (η_{cc} ~1).[19]

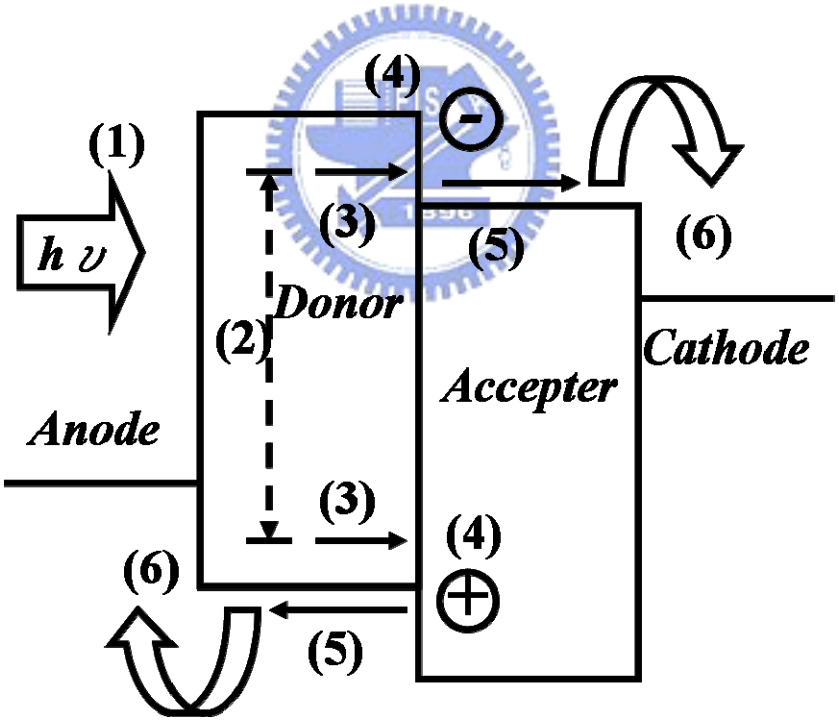

Figure 1.7 Schematic illustration of the continuous steps in photocurrent generation of OPV devices: (1) light absorption, (2) exciton generation, (3) exciton propagation to the D/ A interface, (4) electron and hole (charge carriers) dissociation, (5) charge carriers transportation, and (6) charge carriers collection by the cathode and anode.

The absorption of chemical materials is based on the Beer-Lambert Law : $I = I_0 \times 10^{-\alpha L}; \alpha = \frac{4\pi k}{\lambda}$, where k is the extinction coefficienct, λ is the wavelength of the light, α is the absorption coefficienct, L is the distance that the light pass through the material, and I, I_0 are the initial and final intensities of light, respectively. In order to get high absorption efficiency, L should be thick enough to harvest most of the solar irradiance. However, a thick L causes lower exciton diffusion efficiency and reduced carriers' transportation efficiency. To increase light absorption and to decrease L, a metal cathode (Al) is used in the OPV device due to the former's high reflectivity. Moreover, an anti-reflection coating can be used to increase light absorption owing to the reduction of surface reflection.

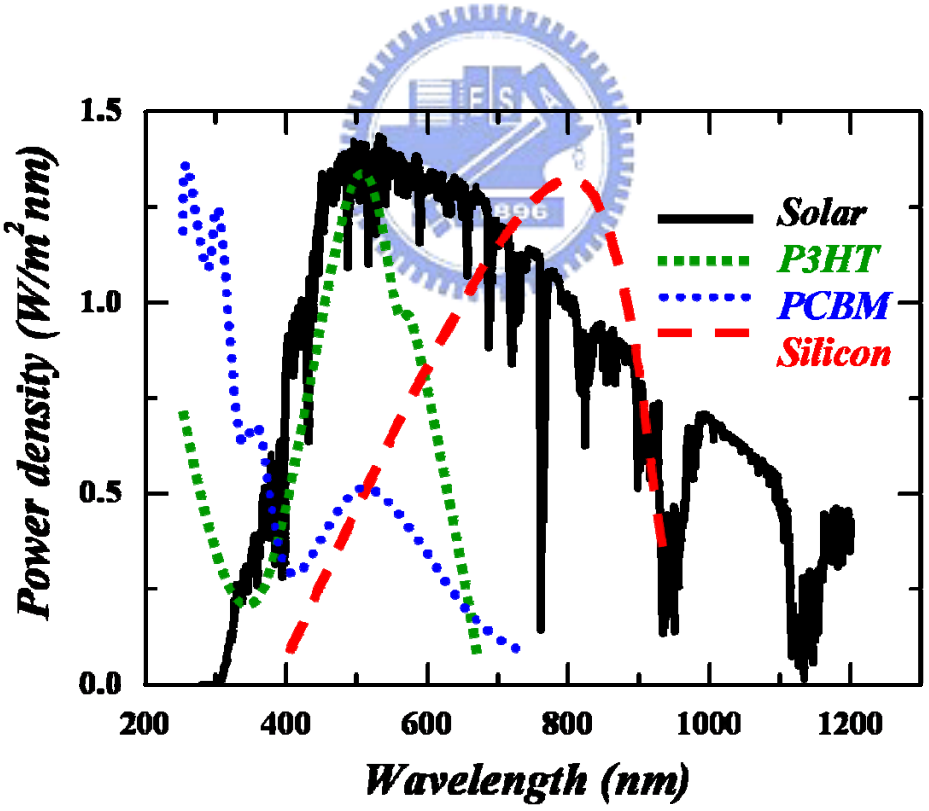

Figure 1.8 A normal incident solar spectrum at sea level on a clear day and the absorption spectra of P3HT, PCBM, and silicon. The wavelength range is between 200 and 1500nm.

Figure 1.8 shows the solar spectrum at sea level on a clear day and the absorption spectra of P3HT, PCBM, and silicon, respectively. It can be seen that the spectrum of the solar irradiance is broad which includes UVA (320-400nm), visible light (400-700nm), and IR regions. The peak wavelength of solar spectrum is located at 500nm (green light). Similarly, the absorption spectrum of P3HT mainly ranges from 300 to 650nm, which matches well with the peak irradiation of the solar spectrum to achieve high absorption efficiency. In contrast, the absorption spectrum of inorganic materials (i.e. silicon and GaAs) ranges from visible light to near IR due to their lower band gap. To make full use of solar energy, different active layer materials are used in OPV devices to absorb the power that associate to their band gaps.[20, 21]

1.5 Motivation and objective of this dissertation

Numerous techniques have been adopted to fabricate MLAs, for examples, photoresist reflow and etch transfer,[23] ink-jet printing (IJP),[24, 25] laser ablation,[12] direct laser-writing,[11] and gray-scale mask lithography.[26] However, each of the aforementioned methods still has its own drawbacks. For instance, the reflow method requires high process temperature and a complicated etch transfer process. Furthermore, limitation in lens-size and alignment accuracy makes IJP undesirable. For laser ablation, one has to face the problems of high facility-cost and high energy consumption. For direct laser writing, the surface roughness of lens presents a problem. Although gray-scale mask lithography eliminating etch-transfer from the traditional lithographic approach, it is difficult to fit the desired shape precisely and to distinguish the gray-levels in a sharp edge. In this dissertation, a simple and cost-effective fabrication method of self-organized microlens arrays is proposed using spin-coating or ink-jet printing on self-assembled monolayer pre-patterned substrates.

OLEDs can be used for commercial applications such as screens for mobile phones, portable digital-audio players, car radios, digital cameras and high-resolution micro-displays. The internal quantum efficiency (η_{int}) of OLED is defined as a ratio of the number of photons produced within the device to the number of injected charge carriers. Subsequently, the external quantum efficiency (EQE) of OLED is defined as a ratio of the number of photons observed being observed outside the device to the number of charge carriers being injected into the device. As a result, the relationship between EQE and η_{int} is represented as $EQE = \eta_{cp} * \eta_{int}$ where η_{cp} is the out-coupling efficiency. The refractive indices of glass substrate, ITO, and organic materials are 1.5, 1.8, and ~1.7, respectively. Therefore, most of the generated light is trapped in the substrate, ITO, and organic layer due to the total internal reflection (TIR). Only the external mode (incident angle smaller than critical angle) is observed. In this context, the η_{cp} based on the calculation using ray optical method is only 20%. Many approaches have been proposed to increase the η_{cp} of an OLED, such as making a rougher front-surface, adding a diffusion layer, or incorporating an index-matched material. In this dissertation, a method is proposed to enhance the out-coupling efficiency of PLEDs incorporated with self-organized microlens arrays.

Since C. W. Tang[27] revealed his high performance organic photovoltaic (OPV) devices in 1986, researchers have been involved this field ever since. The OPV devices use copper phthalocyanine (CuPc) and perylene tetracarboxylic derivative (PA) in a bilayer structure and its power conversion efficiency (η_p) has increased to 1%. N. S. Sariciftci[28] and coworkers demonstrated OPV devices based on a blend of MDMO-PPV and PCBM (1:4 by weight) as the organic active layer in a bulk-heterojunction structure. The η_p increased to 2.5% because of the improvement of charge-carriers dissociation efficiency. They also showed that thermal-annealing

enhances the phase-separation of the donors and accepters;[29] therefore, the electron- and hole-mobility are enhanced and become more balanced. F. C. Chen et al.[30] demonstrated that the modification of PEDOT: PSS reduces the series resistance of OPV devices effectively. As a result, the mobility and photocurrent were increased and led to 5.2% power-conversion efficiency. The evaluation of the performance of an OPV usually requires a solar simulator (air mass 1.5) in a laboratory at room temperature. However, the solar irradiance changes dramatically with time and weather. In addition, the temperature of OPV devices varies with the thermal transformation in practical operating situations. In this dissertation, the performance of OPV devices operated under various conditions of illumination and temperature will be investigated in order to optimize their performance. Moreover, a method to enhance the use of solar irradiance using light-collecting systems is also proposed.

1.6 Organization of this dissertation

The following is the outline of this dissertation. Chapter 2 presents the fabrication process of micro-contact printing, a self-organized microlens array, an organic light-emitting diode, and an organic photovoltaic device. The fabrication of a self-assembled microlens array using hydrophobic effects is presented in Chapter 3. Chapter 4 and Chapter 5 examine the enhanced light out-coupling efficiency of polymer light-emitting diodes using spin-coated and ink-jet printed microlens arrays, respectively. In Chapter 6 the performance of organic photovoltaic devices under diverse operating conditions is evaluated. Finally, in Chapter 7 discussion and summary of the dissertation, including the recommended future works, are presented.

Chapter 2 Experimental Methods

2.1 Introduction

This chapter describes the process involved in the fabrication of silicon molds, PDMS stamps, self-assembled monolayer (SAM), self-organized microlens array (MLA), polymer light-emitting diodes (PLED), and organic photovoltaic (OPV) devices.

2.2 Fabrication of silicon molds and PDMS stamps

The fabrication process of a silicon mold was based on a photolithographic procedure. First, a silicon wafer was cleaned using RCA procedures. Then, the photoresist (PR) was spin-coated on the wafer and pre-baked at 90 °C for 1 minute. After being covered by a photo-mask and exposed to ultraviolet (UV) light irradiation, the pattern of the photo-mask was transferred to the PR. Next, the unprotected area of the photo-resist was removed using PR-developer. Finally, after post-baking at 120 °C for 1 minute, the wafer was etched using a reactive-ion-etch (RIE) and to form a silicon mold.

Stamps used in micro-contact printing (μCP) are made of poly(dimethylsiloxane) (PDMS, Dow Corning Sylgard Elastomer 184) and are replicated from the silicon mold resulting from the photolithographic process. First, the silicon mold is dipped into an anti-adhesion solution, which is made of trichloro(3,3,3-trifluoropropyl)silane (Aldrich) dissolved in propylene glycol monomethyl ether acetate (PGMEA) at a concentration of 1mM. After baking at 100 °C for 2 minutes, the anti-adhesion layer of low surface energy is formed on the mold. A blending of PDMS and 10% reagent is fully disturbed and then is poured onto the mold. The mixture is solidified after baking at 60 °C for 1 hour. The PDMS stamp and mold separated due to the effect of

anti-adhesion layer.

PDMS is used as the material for the stamp for the following reasons: first, it has low surface energy and good chemical stability. Second, it is porous such that gas passes easily through it without causing swelling with humidity. Third, it has good thermal stability and high optical transparency in the full range of visible light. Fourth, the prepolymer state of PDMS is liquid at room temperature and becomes solid only after cross linking. Fifth, PDMS is durable and resists mechanical stress and chemical corrosion. Finally, the surface properties of PDMS can be modified using plasma treatment to produce a wider range of surface energies. However, there are still some drawbacks to PDMS being used as a μCP stamp. First, the stamp shrinks when the prepolymer of PDMS is cured. Second, the stamp deforms when the aspect ratio of the microstructures in PDMS is too high or too low and after it sustains the force of contact printing. These problems need to be solved in order to achieve a precise pattern-transfer for large-area μCP applications.

2.3 Micro-contact printing

Due to its high level of stability and reliability, photolithography is a traditional micro-fabrication method used in industries and laboratories The fabrication process associated with photolithography is quit complicated; it includes (in the following order) depositing, photoresist (PR) coating, soft baking, exposing, developing, hot baking, etch transferring, and PR striping. The resolution of photolithography is determined by the wavelength of the light exposure such as G-line, I-line (365nm), and deep-UV line (e.g. 248nm XeF or 193nm ArF excimer laser). However, there still exists a fundamental limitation with this process and that is the feature size has to be at least 100nm owing to the diffraction and short wavelength cutoff of its optical elements. Other lithographic approaches have been developed to overcome this

limitation, such as extreme UV (EUV) lithography, soft X-ray lithography, e-beam writing, and focused ion beam (FIB) writing. Although, these alternatives are very expensive and difficult to acquire, efforts should be made to use them in mass-production because of their superior resolution.

Micro-contact printing (μCP) is another option for micro-fabrication which offers advantages over the previously mentioned alternatives. It uses a patterned elastomer stamp rather than a rigid photomask which is used in photolithography. The advantages for using μCP as a micro-fabrication method include a simpler fabrication process, a lower facility cost, and a wider range of application surfaces. Most importantly, the μCP can be applied to curved surfaces and be used with a wide variety of materials and surface properties.

Currently, a PDMS stamp with relief structures is used in μCP to adsorb the ink in order to form the patterns of self-assembled monolayer (SAM) on substrates. The general form of SAM is $Y(CH_2)_nX$, where Y is an anchoring group used to bind with the substrates and X is a heading group to replace the surface properties of the substrates. The best-established systems of SAM are those of alkanethiolates on gold and alkylsiloxanes on SiO_2 or glass. The reaction of alkanethiolates (in solution or as vapor) and gold occurs with the loss of dihydrogen and when a chemical bonding between S (sulfur) and Au is formed (covalent bonding). The alkyl chains extend from the surface and are tilted at approximately 30° from the normal to the surface to maximize the van der Waals interactions between the adjacent methylene groups.

In this dissertation, the SAMs of alkylsiloxane are formed on transparent glass substrates using μCP. The chemical structures of the precursor molecules of SAM are Octadecyl-trimethoxysilane (OTS, Fluka) and 1H, 1H, 2H, 2H perfluorooctyltrichlorosilane (FOTS, Fluka) which are shown in Figure 2.1(A) and

2.1(B). After μCP the ink of precursor molecules on the glass substrates, SAM of organosilane form on the hydroxyl OH-bearing surface as a result of the chemical reaction between the organosilane molecules and the OH sites on the surface. Consequently, a condensed organo thin-film forms to replace the physical and chemical properties of glass substrates, as shown in Figure 2.1 (C).

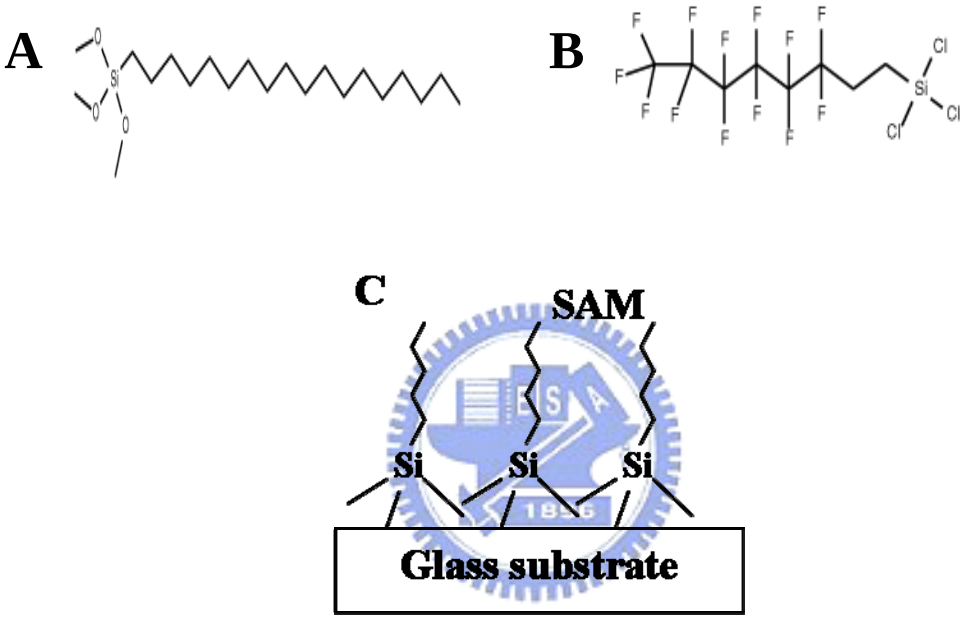

Figure 2.1 Chemical structures of SAM, (A) OTS and (B) FOTS, used in this dissertation. The SAM deposits on the glass substrate and covalent bonding is formed. The surface properties of the substrate are substituted by the functional groups of SAM.

The patterned SAMs are suitable as resistors in selective wet etching if a suitable aqueous solution is selected. It can be applied to micro-fabrications to replace the traditional lithographic process due to the simple and cheap procedure. In addition, we can use the substrate with patterned SAMs as templates in selective deposition. For

example, the surface property of glass is intrinsic hydrophilic and becomes hydrophobic after the patterns of SAMs of organosilane formed using μCP. After dipping the substrate into water or prepolymer solution, the liquid selectively dewetted on the hydrophobic regions and trapped on the hydrophilic regions. In contrast, organic materials are intrinsic hydrophobic and are selectively deposited on the hydrophobic surface as selective nucleation. The self-organization phenomena can be used to fabricate polymer optical elements (such as microlens arrays) or electronic devices (such as organic thin film transistors, organic solar sells, and liquid crystal displays etc.)

2.4 Fabrication of a self-assembled microlens arrays

The fabrication process of the mold and the microcontact printing (μCP) stage are illustrated in Figure 2.2. The photoresist was spin-coated on a silicon wafer with 2μm film thickness and then developed by 2.5% tetramethylammonium hydroxide (TMAH). The patterns of photoresist were circles with 50, 75, and 100μm in diameters and 5, 10, and 15μm in spacing. In a typical selective surface treatment experiment, the PDMS stamp was immersed in a solution of 1H, 1H, 2H, 2H - perfluorodecyltrichlorosilane (FOTS) dissolved in heptane (1mM) for 30sec. After being removed from the solution and dried under a stream of nitrogen, the stamp was brought into contact with a UV-ozone treated glass substrate for several seconds and the force applied during the contact was 0.2N. The UV-ozone treated glass substrate showed high wettability such that the contact angle (CA) was smaller than 5 degrees; the FOTS formed a self-assembly monolayer (SAM) with extremely low surface energy such that the CA was greater than 110 degrees. As a result, the surface properties of the substrate were divided into a hydrophilic region on the bare glass and a hydrophobic region on the SAM treated surface. The substrate was then spin coated

with a prepolymer solution NOA65 (Norland Optical Adhesive 65, THORLABS INC.), an index matching material. Consequently, the NOA65 was swept away on the SAM modified surface because of poor adhesion on the hydrophobic regions and then self-organized as microlenses with hemisphere structures by the surface-tension effects. Finally, the microlenses were completed by UV-curing.

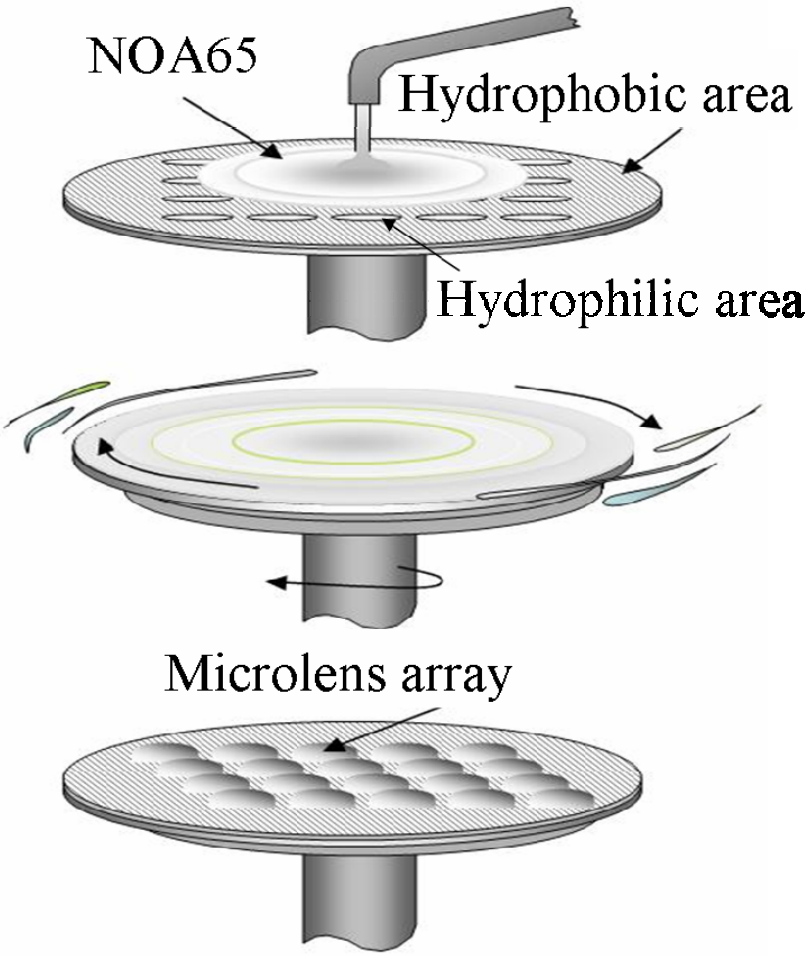

Figure 2.2 Fabrication process flows of the MLA. The pattern of the hydrophobic region was firstly defined by microcontact printing of SAM. The unmodified regions (the circle areas) remained hydrophilic. After spin-coating the prepolymer solution onto the substrate, the microlenses were self-assembly in the hydrophilic regions. Finally, the MLA was completed with UV-light curing.

2.5 Fabrication of polymer light-emitting diodes

A polymer light-emitting diode was fabricated using polyfluorene. (PF, MW=50000, purchased from American Dye Source) The device structure of PLED was ITO (150nm) / PEDOT: PSS (80nm) / PF (100nm) / Ca (30nm) / Al (100nm). The ITO anode was patterned by a photolithographic procedural and then treated by UV-ozone. Then, an aqueous dispersion of PEDOT: PSS (Baytron® P VP Al 4083) was spin-coated at 4000rpm and baked at 80 °C for 1hour. After that, the PF was spin coated at 2000rpm and baked at 100 °C for half an hour in a grove box. The cathode defined by a shadow mask was thermally evaporated under $6x10^{-6}$ Torr in a vacuum chamber and the deposition rate was about 5Å/sec.

2.6 Fabrication of organic photovoltaic devices

The device structure of OPV devices is composed of P3HT/PCBM blend sandwiched between a transparent anode and a metal cathode. The anode consisted of a glass substrate coated with a 100nm indium tin oxide (ITO) film and a 30nm modification layer, PEDOT: PSS (Baytron® P VP Al 4071). A 100nm blend of P3HT: PCBM (1: 1) was spin-coated on the substrate of anode in a nitrogen-filled glove box. The device was covered with a dish over night to slow down the evaporation rate of solvent and then annealed at 120 ℃ for 10 minutes. The device was completed with the placement of a 10nm Ca and 100nm Al cathode, which was thermally evaporated under a pressure less than 10^{-6} Torr (1Torr ~ 133Pa). The current density-voltage (*J-V*) characteristics were measured using a Keithley 2400 source meter unit (SMU) while the solar cells were illuminated by an Oriel Solar Simulator (AM 1.5G). The illuminations of light source varied from 0.28 to 10.0 (kW/m^2) depending on the neutral-density filter used and was calibrated by a silicon photodiode S1133 (Hamamatsu). The temperature of the device was changed from 277 to 357K using a

heater and calibrated by a thermal couple. The polymer heat-flows were estimated using a differential scanning calorimeter (Diamond DSC, Perkin Elmer).

Chapter 3 Fabrication of self-assembled microlens arrays using hydrophobic effects

3.1 Introduction

Among the methods of MLA fabrication, one interesting approach is using the hydrophobic effects. This method is based on self-assembly of liquid prepolymer due to the repellence of hydrophobic patterns on substrates. The techniques used in the creation of patterns include micro-contact printing (CP) of self-assembled monolayers (SAM)[31, 32] and adhesive lithography.[33, 34] This provides a much simpler method to fabricate MLAs using the hydrophobic effect. However, the major disadvantages involve the attachment of the lens-material on the reverse side of the substrate and it is difficult to apply to a large area. In this work, the self-assembly phenomena of microlens arrays caused by the so-called "spin-coating-assisted hydrophobic effect" on glass substrates are presented. The operation parameters of the spin-coating process, such as the spin rate, provide another dimension to control the lens shape. In addition, in contrast to the dip-casting method, spin coating is a more reliable and popular method used in laboratories and industries. Only one side of the substrate is coated in the spin-coating process and the other side can be keep clean. The new approach reported in this letter provides a simple, low-cost and mass-production approach to fabricate MLAs.

3.2 Surface properties of SAM-treated substrates

To prepare the substrates with different wetting ability, the glass sheets either were dipped into SAMs of OTS and FOTS, or underwent UV-ozone treatment. Table 3.1 lists the surface energy of the substrates with the three different kinds of surface treatments. It clearly shows that the surface energy of the glass substrates decreases to

27.3 and 12.5 (mJ/m^2) after OTS and FOTS treatment, respectively. The lower surface energy means that the surface is more hydrophobic and, therefore, that the hydrophilic liquid will not easy condense on it. On the other hand, the surface energy increases to 47.68mJ/m^2 after UV-ozone treatment. The contact angle (CA) reduces to less than 5 degrees, which means the glass substrates become more hydrophilic.

Table 3.1 Contact angles and surface energies of glass substrates treated with UV ozone, OTS [a], and FOTS [b]

Surface treatment of substrates	Contact angle (degree)			Surface energy (mJ/m2)
	Water	Diiodomethane	Ethylene glycol	
UV Ozone	5.0	39.9	6.6	47.68
OTS[a]	87.4	50.8	75.3	27.31
FOTS[b]	105.1	91.5	92.5	12.47

[a]Octadecyl-trimethoxysilane

[b]1*H*,1*H*,2*H*,2*H*-Perfluorooctyl-trichlorosilane

Figure 3.1 shows the images of water drops on the three differently-treated surfaces. The CA values of FOTS- and OTS-treated surfaces are higher than that of UV-ozone-treated surface. The glass substrates treated with both FOTS and OTS clearly demonstrate their unique dewetting ability with respect to NOA65. Furthermore, FOTS shows the better dewetting ability owing to the fluorine contained molecule. In fact, the film with molecules with fluorine atoms have been used to serve as the anti-adhesion layer for hot embossing system[35, 36] or UV-curing system.[37] To reduce the adhesion of the prepolymer, NOA65, we chose FOTS as our alignment layer to confine the prepolymer (NOA65) after the spin coating process.

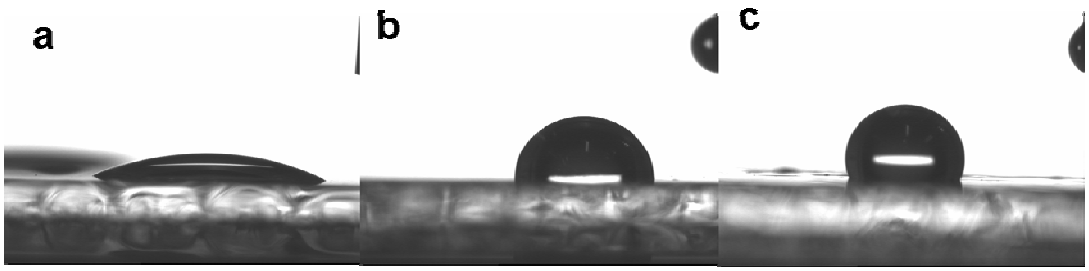

Figure 3.1 Drop images of water on glass substrates with surface treatments of (a) UV-ozone (b) OTS (c) FOTS, respectively.

3.3 Results and discussion

Figure 3.2 reveals the as-fabricated MLAs with different sizes from 50μm to 100μm after spin-coating and UV-curing of NOA65 on the glass substrate. The lens size and shape corresponds well to the pattern of the mold used in the micro contact printing. In addition, the well-defined pattern of lenses also shows the priming layers (SAM) are printed on the surfaces without any mold deformation during imprint process. Finally, the surface around the lenses is nearly flat and without any residual materials (NOA65) due to the poor adhesion force. The residual NOA65 might introduce the light scattering, which would degrade the performance of the MLA, while light passes through the glass substrates.

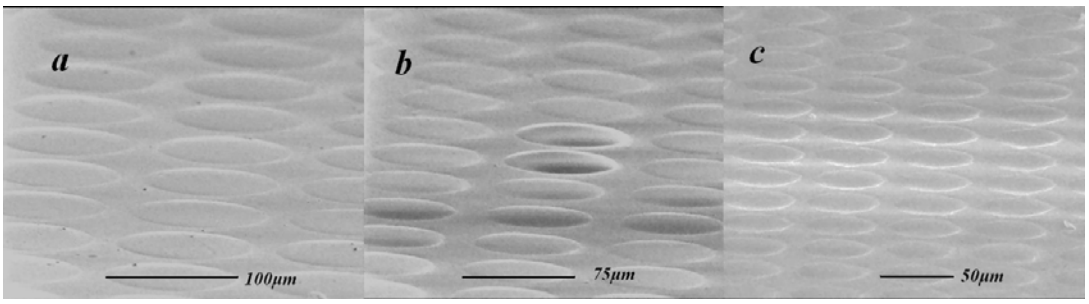

Figure 3.2 Vertical view images of microlens arrays obtained on a scanning electron microscope (SEM). The diameters of microlenses are (a) 100μm, (b) 75μm, and (c) 50μm.

The parameters of lens shape, such as the radius of footprint (r) and sag-height (h), were obtained from the measurement of interferometer as shown in Figure 3.3(a). The lens-profile, which is obtained on an alpha-step p-1 profilometer (KLA-Tencor Corporation), shows a smooth surface as the inset of Figure 3.3(b). The surface roughness is less than 1 nm from the surface analysis by an atomic force microscopy. In addition, the measured lens-profile is also very similar to the simulated one, implying high quality of the lenses. The measured lens diameter is exactly identical to that of the dimension of a circle designed on the PDMS mold, which implies that precise pattern transfer has been achieved with this method. In addition, one can also observe that perfect plano-convex lenses were formed in the hydrophilic regions due to a minimum surface-energy of the prepolymer. Moreover, the well-defined pattern with distinct boundary indicates that the hydrophobic SAM can effectively repel the adhesive prepolymer liquid on the FOTS-treated regions. The difference in contact angles of NOA65 between the hydrophobic and hydrophilic regions is more than 60 degrees, indicating that a large surface energy difference is created by the surface structure. The large difference in surface properties between the two regions is actually one of the keys to obtain high quality MLAs.

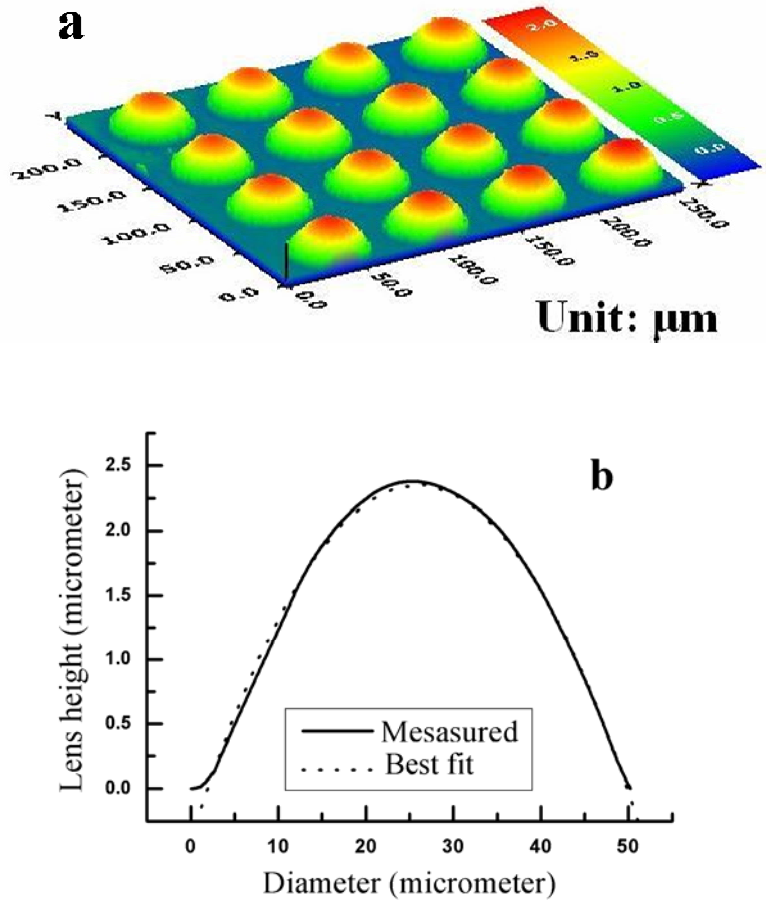

Figure 3.3 (a) Vertical view images of microlens arrays obtained on an interferometer. (b) Cross section of a microlens of 50μm-diameter obtained on an alpha-step.

For a thin planar-convex lens, the focal length (*f'*) and *f-number* ($f_{\#}$) can be calculated using the following relations:

$$R = \frac{h^2 + r^2}{2h}, f' = \frac{R}{n-1}, f_{\#} = \frac{f'}{2r}$$

where R is the curvature radius of the lens surface, and n is the refractive index of the lens material (n=1.524 for NOA65). For example, the $f_{\#}$ is 5.14 for a lens with a 50μm diameter and 2.34μm sag-height. The relationship between the $f_{\#}$ and the fill factor (FF), that is the area-ratio of a microlens to a pixel, is illustrated in Figure 3.4(a). It can be seen that the $f_{\#}$ decreases with a decrease in the FF. This suggests that more lens material is gathered in the smaller hydrophilic region to form a stronger (lower $f_{\#}$)

microlens when the FF is smaller. In other words, the greater amount of NOA65 is repelled to the UV-ozone-treated areas, the stronger lenses are formed.

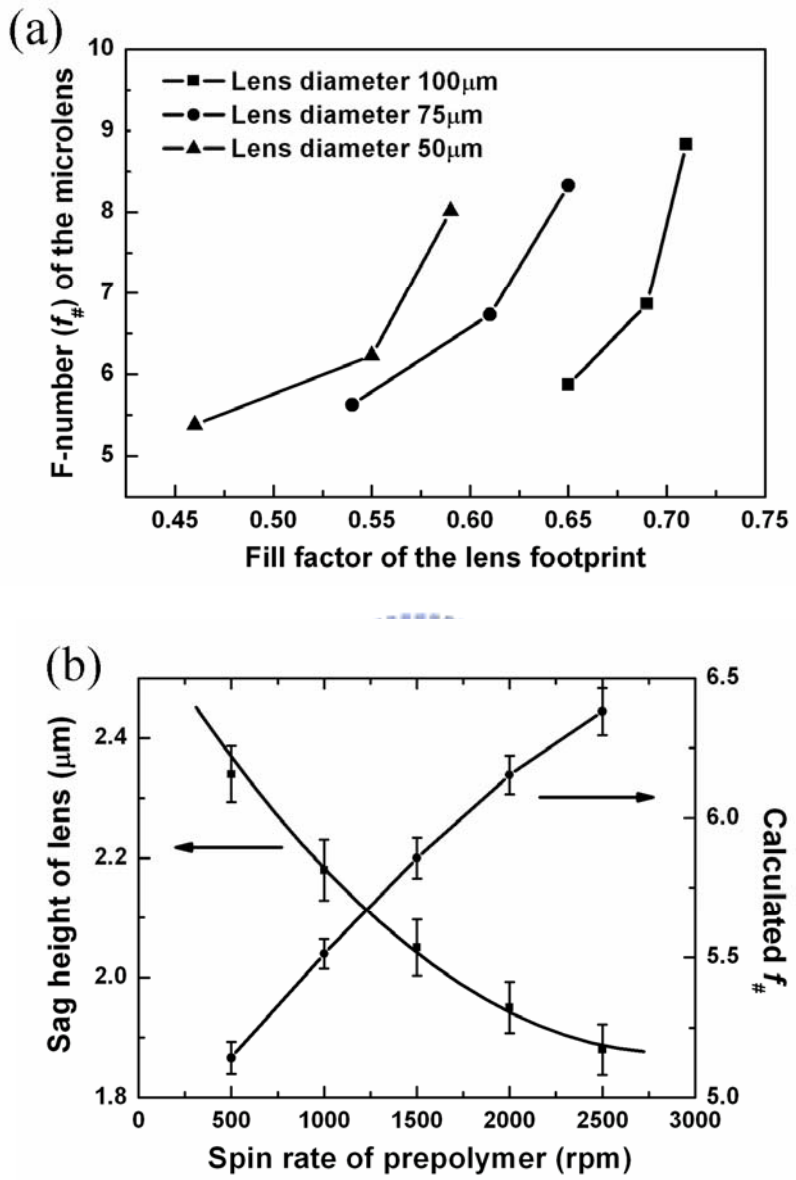

Figure 3.4 (a) The $f_{\#}$ depends on the fill factors of MLAs. The lens diameters are 50, 75, and 100μm with 5, 10, or 15μm spacing. Different FF was obtained from the MLA with the same diameter but different spacing. (b) The corresponding sag-heights (h) and calculated f-number ($f_{\#}$) of MLAs versus spin rates of the prepolymer coating. The lens diameter is 50 m.

However, the $f_{\#}$ is not only determined by the FF but also by the spin rates, which is an easily-controlled parameter. To further investigate the effect of spin-coating process on the properties of MLAs, different spin rates were used to fabricate the MLAs. Conventionally, the polymer film thickness (t) was evaluated by the following empirical equation:

$$t \propto s^{-1/2} v_0^{1/3}$$

where s and v_0 are the spin rate and the initial viscosity of the polymer, respectively. Figure 3.4(b) illustrates the relationship between the lens sag-heights (h) and the corresponding spin rates. The data shown also fits well within the above empirical equation. As the spin-rate decrease from 2500 to 500 rpm, the lens sag-height increase from 1.89 to 2.34 m. The $f_{\#}$ of microlens as a function of the spin rates is also presented in Figure 3.4(b) and ranges from 5.14 to 6.38. The results demonstrate clearly that the lens sag-heights can be completely controlled by the spin-rates. In addition, for the uniformity of microlens arrays, as shown in Figure 3.4(b), the average derivation of focal length $\Delta f'/f'$ is less than one percent at 1000 rpm, implying a high level of uniformity.

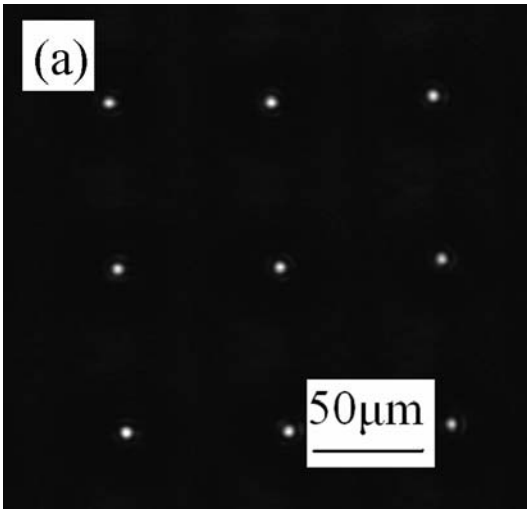

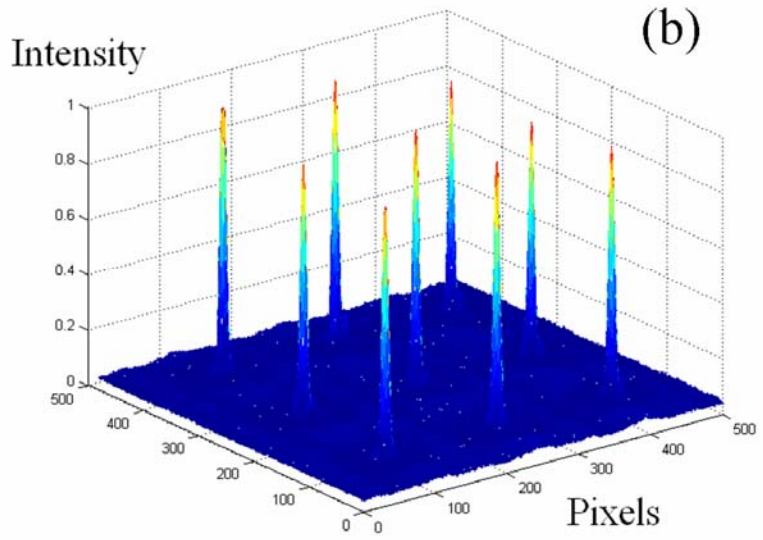

Figure 3.5 (a) Focused light-spots image of a MLA on the focal plane. The lens has a 50μm diameter and 15μm spacing. (b) 3D energy distribution of light-spots

A configuration of 100 by 100 MLA (each lens with 50μm in diameter and 15μm in spacing) has been successfully developed. The focusing property of the MLA is also evaluated by a beam profiler. Figure 3.5(a) shows the image plane produced by a collimated laser beam illuminated through the MLA. The focused light-spots demonstrate the strong focusing ability and the high uniformity of the MLA. Figure 3.5(b) shows a 3D energy distribution of light-spots. This energy distribution reveals a high level of uniformity from one light-spot to another because the deviation of the energy peak is smaller than 10 percent. The FWHM (full width half maximum) of the light spots measured from the cross sectional view is 4.95 ± 0.25μm, which is very close to its theoretical value. These data suggests that a high-quality MLA has been fabricated.

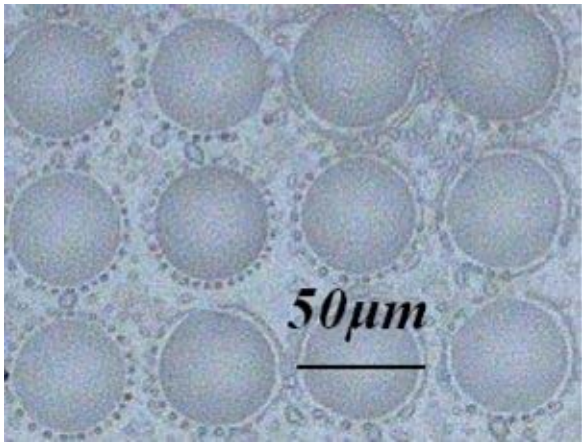

Figure 3.6 Microlens array fabricated on a PES substrate. The lenses have a 50-μm diameter and 15-μm spacing.

The method presented here is quite unique from several aspects. First, the spin-coating is adapted instead of the complicated lithography and reflow methods to fabricate MLAs. It is clearly a more efficient and practical approach for high-volume production. Second, instead of using gold for CP of the SAM with alkanethiolates, glass is used as the substrate material. The high transparency of the glass substrate ensures minimum the reflection and absorption of light. Furthermore, the NOA65 is an index-matched material which can reduce the reflection at the lens-substrate interface and the absorption is low in the range of visible light. Finally, the UV-ozone treatment is used to obtain a hydrophilic surface. This process not only makes the substrate hydrophilic by chemically oxidizing the surface but also provides the oxygen moieties for the formation of covalent bonds between the substrate and the organosilanes. Consequently, a variety of substrate materials may be used, as long as they can be oxidized. For example, Figure 3.6 demonstrates that the MLA was fabricated on a polymer substrate, PES (Polyethersulphone). This feature is quite important for the future development of flexible display technology, since MLAs on flexible substrates can be integrated into them directly.

3.4 Conclusion

In conclusion, one fast, low-cost, low-temperature and profile-controllable approach has been demonstrated to fabricate polymer microlens arrays. By the simple process of microcontact printing and spin-coating, the microlenses become self-assembly on the SAM treated glass substrates. The demonstrated MLAs are made of NOA65 prepolymer with lens sizes of 50, 75, and 100μm in diameter. The microlenses have $f_{\#}$ ranging from 5.14 to 8.83, depending on the lens diameters and the spacings. Lens shapes can be controlled by changing the spin rates of prepolymer coating. Lens profile of MLA obtained on the interferometer and alpha-step shows good surface roughness and uniformity. Finally, optical measurements have demonstrated an excellent light-collecting capability from the fabricated MLAs.

Chapter 4 Enhanced Light Out-coupling Efficiency of Organic Light-emitting Diodes Using Self-organized Microlens Arrays

4.1 Introduction

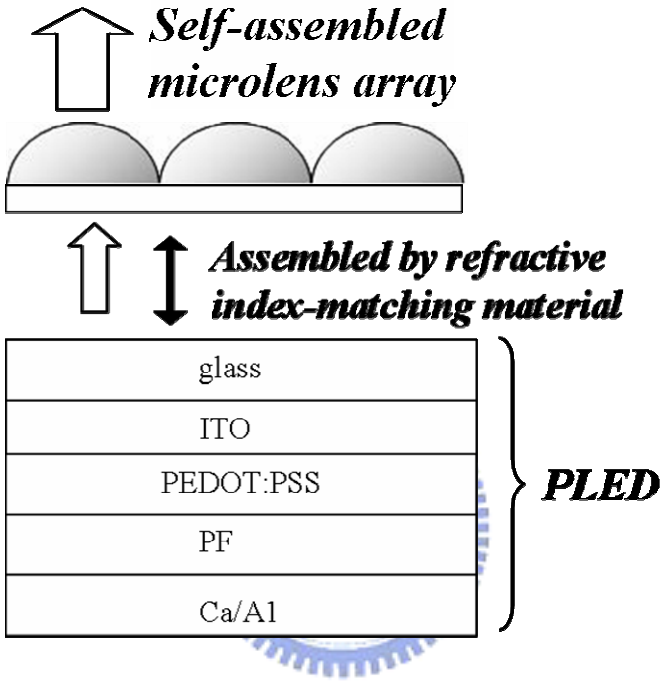

Figure 4.1. Device structure of a PLED incorporating with a MLA. The light emitting from the device is enhanced by the MLA.

Due to the high power efficiency and simple fabrication processes, organic light emitting diodes (OLEDs) are the focus of attentions in the applications of display.[38, 39] However, the out-coupling efficiency of OLEDs is limited because the total internal reflection (TIR) happens at the substrate-air interface. Some methods have been presented to improve the light out-coupling efficiency, such as coating an index-matched material on the substrate[16] or by adding a distributed Bragg reflector.[40] In addition, microlens arrays (MLAs) have been used to increase the critical angle of the surface and to reduce the microcavity and waveguide effects.[18]

However, these methods require either complicated processes or expensive facilities. In this work, we demonstrate here a new fabrication method to make a self-organized MLA on a polymer-based OLED (Figure 4.1).[41, 42] This method provides an easy way to make micro-optical components. After incorporating the MLAs into an OLED, the optical measurement showed that the luminance of OLEDs with MLAs was improved by 24.5% without any apparent color-change. Furthermore, all fabrication steps can be accomplished in an ambient environment and at room temperature. It is anticipated that this method has great potential for mass replication.

4.2 Proposed methods

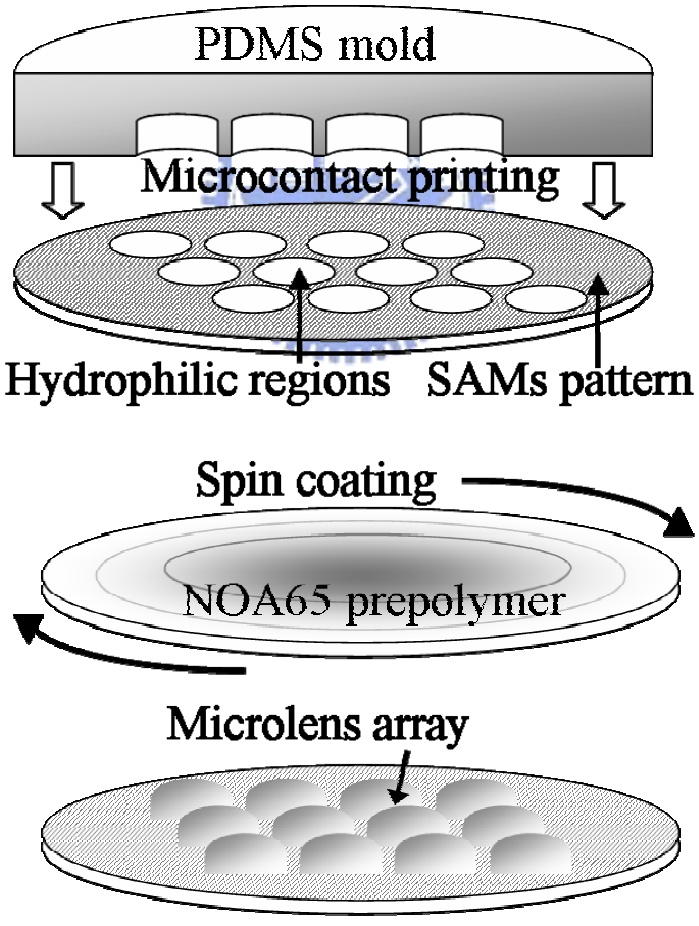

Figure 4.2. Fabrication processes of a self-organized microlens array. The substrate was defined by microcontact printing of hydrophobic SAMs. After spin coating of NOA65 prepolymer, the MLA was formed and then solidified by UV-curing.

The fabrication processes of microlens arrays (MLAs) are illustrated in Figure 4.2.[41, 42] The surface of the substrate was patterned into hydrophilic or hydrophobic regions by microcontact printing of the self-assembled monolayers (SAMs).[43] The hydrophobic region was defined by microcontact printing of SAMs (1H, 1H, 2H, 2H-Perfluorooctyl-trichlorosilane, FOTS). After spin coating (spin rate 1500rpm) the prepolymer solution NOA65 (Norland Optical Adhesive 65, THORLABS INC.), an index-matching material, on the glass substrate, the microlenses became self-organized on the hydrophilic regions. Because NOA65 is intrinsically hydrophilic, the lens material was then swept away in the spin-coating process on the hydrophobic region, which is covered by the SAMs. Following the pattern, NOA65 became plano-convex microlenses on the un-coated surface due to the much stronger adhesive force. Finally, the microlenses were completed by UV-light curing. The MLA was brought into contact with an OLED and adhered to the glass substrate of the OLED using NOA65, the refractive index-matching material.

4.3 Results and discussion

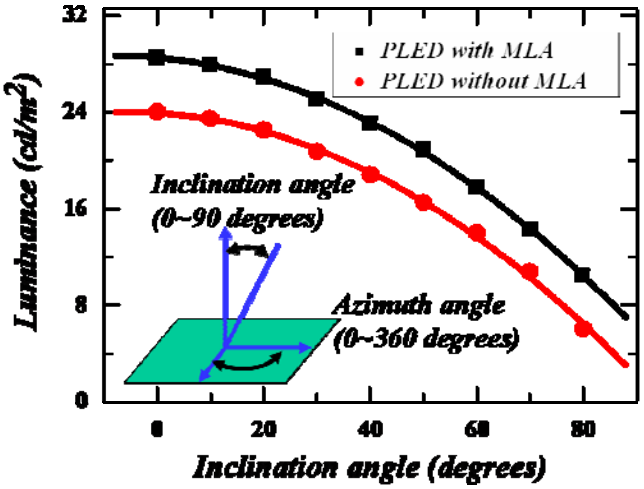

Figure 4.3. Inclination angles dependent luminance of PLEDs with and without MLAs

The viewing angles dependent luminance of OLEDs obtained on a ConoScope ™ (autronic-MELCHERS, GmbH) is shown in figure 4.3. The samples were put close to the detection head and the near field light emitting characteristics were measured. The luminance of PLEDs with MLAs is enhanced 18.75 ±1.25% at surface normal.

From Fresnel's equation, more than 50% of light generated by organic layers is trapped in the OLED due to the TIR. The trapped light goes back and forth for many times and then either emits from the side walls or is absorbed by the organic materials. When the MLA is attached to the OLED, the light of large incident angle can emit from the front surface because of the modified geometric structure. As a result, the light out-coupling efficiency of the OLED is improved, especially at large viewing angle conditions. The out-coupling efficiency of OLEDs will be better if "stronger" lenses are used. For example, the light emission of an OLED incorporating a hemisphere MLA could be enhanced by 60% based on our preliminary simulation results from Tracepro™.

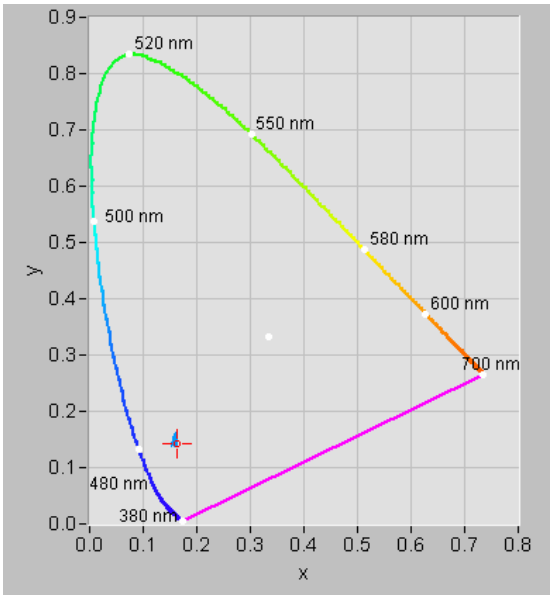

Figure 4.4 Chromaticity of PLEDs with MLAs. The blue dots are color coordinates in different viewing angles associated with the 1931 CIE standard. The red cross-mark indicates the surface normal.

The Colorimetric picture of PLEDs incorporating with MLAs is shown in Figure 4.4. The CIE-coordinate of the light emission from normal direction is x = 0.1628 and y = 0.1428 (the cross-mark in Figure 4.4), which is exactly the same as the one without incorporating the MLAs. The points show the distribution of the CIE-coordinates at all viewing angles of the device. For comparison, the color difference of the luminance between 80 degrees inclination angle and the normal one is calculated as (Δx, Δy) = (0.0056, 0.0008), which is too small to be distinguished by the human eyes.

In this work, the light out-coupling efficiency of OLEDs was improved by more than a factor of 1.2 on average after incorporating a self-organized MLA. The efficiency could be higher by adding a MLA with a smaller $f_{\#}$. Moreover, the luminance drops to 86.5% from the surface normal to 60 degrees inclination angle

without the MLA. After the MLA is added, the luminance only drops to 89.3%. In other words, the viewing angle is also enhanced by incorporating the MLAs, especially at large viewing angles (from 45.6% to 60.1% at 80 degrees).

Because NOA65 is one of the index-matched materials for the glass substrate of OLEDs, the optical loss at the lens-substrate interface is minimized. Most importantly, since NOA65 is with 100% solid-content and solidified by UV-light curing, the lens surface should be perfect; that is without any shrinkage as compared to the traditional molding method.[44] In addition, the MLA and OLED were made separately and then adhered together using NOA65, the interference of process can be avoided and the mass production is very feasible.

4.4 Conclusion

In summary, we have demonstrated a new fabrication method of self-organized MLA for OLEDs. The light out-coupling efficiency of the device was enhanced by 18.75 ±1.25% in this study. The enhancement was up to 60% at 80 degrees viewing angle without any obvious color-shift. The lens material (NOA65) is index-matched to the glass substrate of OLEDs and the transparency is more than 93% in visible wavelength. The fabrication processes of the MLA and the OLED are independent and can be coupled by NOA65 easily. Based on the proposed fabrication methods, mass production of high performance OLEDs is possible. Finally, it is anticipated that the self-organized MLAs can also be fabricated on plastic substrates since only low-temperature processes were involved. It potentially can be used to enhance the efficiency of flexible OLEDs in the future.

Chapter 5 Performance enhancement of polymer light-emitting diodes incorporated with ink-jet printed microlens arrays

5.1 Introduction

As the number of the applications of electro-optical systems in our daily lives continues to grow, the role of reflective microlens arrays (MLAs) in enhancing their performance has become more crucial. Therefore, it is important to develop one effective method to achieve the mass production of MLAs. Numerous methods have been revealed to fabricate the MLA effectively for recent years, such as photoresist reflow and etch transfer,[45] hot embossing,[46] laser ablation,[47] and direct laser-writing[11] etc. Nowadays, the development of ink-jet printing (IJP)[48] technology provides another choice to fabricate the MLA owing to the freedom of shape and position control, low lens-material consumption, and simple fabrication process. Moreover, the IJP is an environmental friendly and energy-saving procedure comparing to the fore-mentioned methods. However, it is a challenge to fabricate the MLA of high fill-factor and low f number using the IJP due to the spread of printed droplets. In this study, an approach was presented to fabricate the MLA using IJP on a substrate which is pre-patterned by self-assembled monolayers (SAMs).[32] The main aspect of the proposed method is the use of micro-contact printing of SAMs to confine the extension of ink-jet droplet. Finally, the fabricated MLA was incorporated into a polymer light-emitting diode (PLED) and the optical characteristics were discussed in this study.

5.2 Proposed method

The proposed fabrication process of an MLA is illustrated in Figure 5.1. The stamp used in micro-contact printing (μCP) was made of poly-dimethylsiloxane (PDMS), in particular Dow Corning Sylgard Elastomer 184. A liquid PDMS mixture (silicone elastomer : curing agent = 10 : 1) was poured onto a silicon mold with relief structures. After baking the mixture at 60℃ for 30minutes, the PDMS became solid and was separated from the silicon mold. The ink used in μCP was made of 1*H*,1*H*,2*H*,2*H*-perfluorooctyl-trichlorosilane (FOTS, purchased from Aldrich) diluted in heptane (1mM). After absorbed the ink, the stamp was brought into contact with an UV-ozone treated glass substrate to fabricate the patterns of FOTS. Consequently, the surface of the glass substrate became either hydrophilic (after UV-ozone treatment) or hydrophobic (after FOTS treatment). After the lens material (NOA65, THORLABS Inc.) was deposited on the substrate by ink-jet printing (IJP), the hydrophilic NOA65 was repelled by the FOTS and became convex structures due to its surface tension. Finally, the convex structures were solidified to become a MLA under UV-light irradiation. The fabricated MLA was affixed to the cover glass of a PLED using an index-matching material NOA65 to minimize any loss in optical efficiency. The optical properties of the PLED, such as brightness, viewing angle, and chroma, were evaluated using a photometer (Minolta CS-100) and a conoscope (ConoScope ™ - autronic-MELCHERS, GmbH).

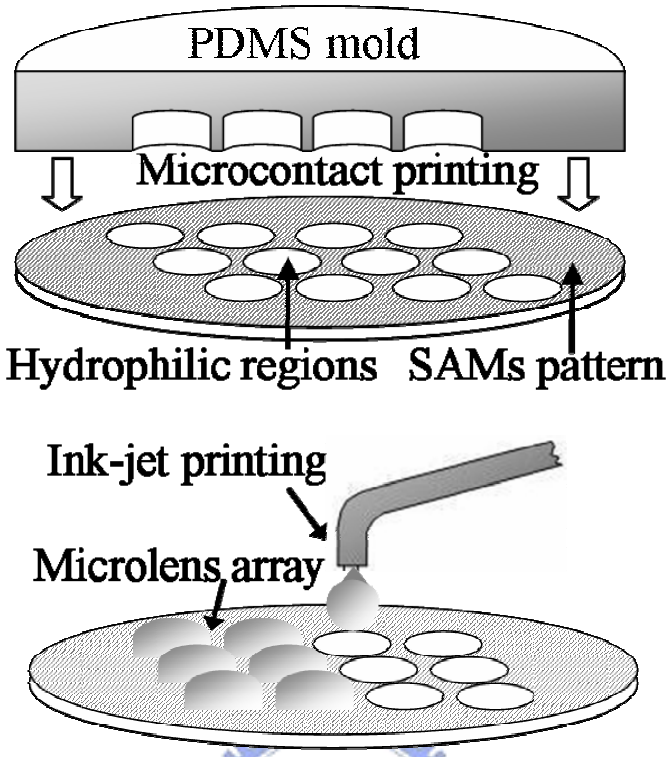

Figure 5.1 The fabrication process of an MLA. After the pattern of the hydrophobic region was defined using micro-contact printing of SAM, the unmodified region remained hydrophilic. After ink-jet printing of the prepolymer (NOA65), the microlenses formed in the hydrophilic regions. Then, the microlenses were solidified using UV-light curing.

5.3 Results and discussion

Figure 5.2(a) shows the profile of a microlens obtained on an alpha-step. The lens-diameter fits the pattern of PDMS stamp very well; it means that the lens-material was repelled by FOTS successfully. Insert of Figure 5.2(a) shows the image of an MLA obtained on a microscope. Figure 5.2(b) shows the morphology of an MLA obtained on a scanning electron microscope (SEM). It can be seen that the MLA has a smooth lens surface and a high level of uniformity in shape. Each lens has a 100μm-diameter with 15μm in spacing, which fits the cavity of the PDMS mold

exactly, implying that a precise pattern transfer has been achieved by this method. The difference in contact angle between the UV-ozone and FOTS treated surfaces is more than 110 degrees, which means that a significant surface energy difference has been created by the two surfaces. The lens-parameters, such as the radius *r* and sag-height *h* of the microlens, were obtained using an interferometer.

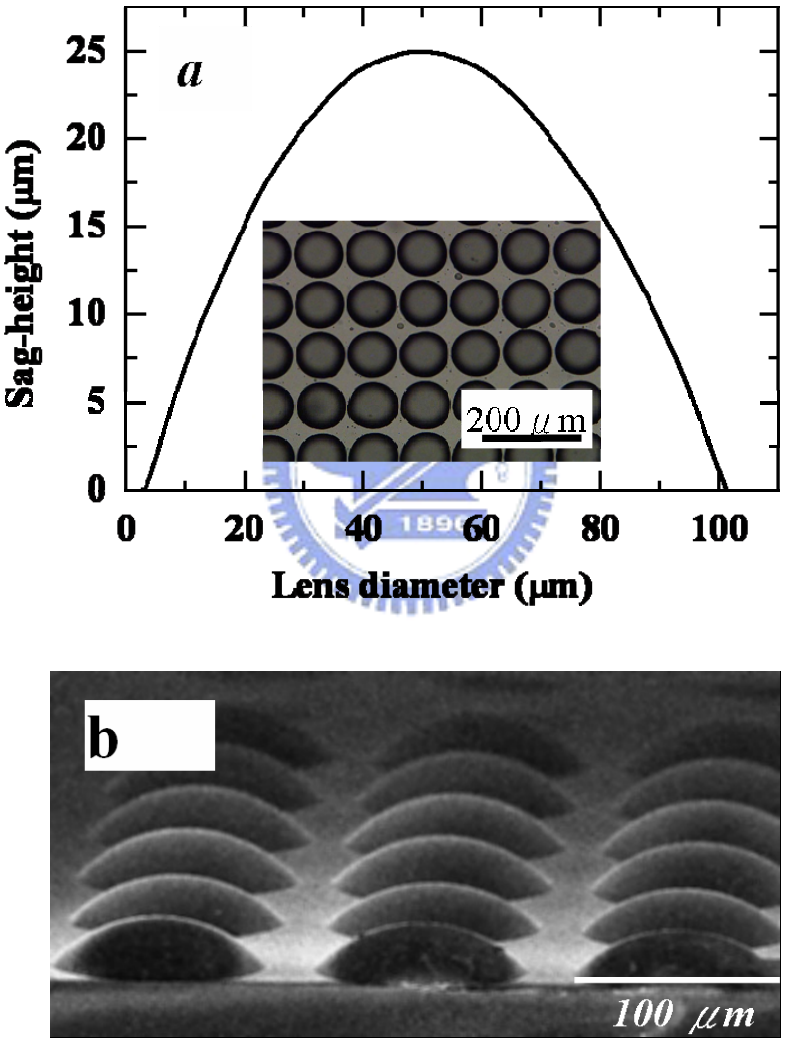

Figure 5.2 (a) Profile of a microlens obtained using an alpha-step. The insert shows the image of an MLA obtained using a microscope. (b) A representation of the morphology of an MLA obtained using a scanning electron microscope (SEM).

Some important parameters of a microlens, such as curvature radius R, focal length f', and f number $F_{\#}$ can be calculated using the following formulas:

$$R = \frac{h^2 + r^2}{2h}, f' = \frac{R}{n-1}, F_{\#} = \frac{f'}{2r}$$

where n is the refractive index of the lens material (NOA65, n = 1.52). The volume of the lens (V), which is a function of R, r and h, can be expressed as:

$$V = \int_{R-h}^{R} \pi(R^2 - y^2)dy = \pi h^2(R - \frac{h}{3}) = \frac{1}{2}\pi h(\frac{h^2}{3} + r^2)$$

The volume of a microlens is determined by the volume of a single droplet (15 picoliter in this study) multiplied by the number of printed droplets. The volume of a droplet is changed according to the diameter of jet-nozzle and the operating voltage of the piezoelectric device. Figure 5.4 shows the h and $F_{\#}$ of a microlens as a function of the volume. The h increases from 20.5 to 26.7μm as the volume increases from 90 to 135 picoliter. The experimental h matches to the calculated h very well and their difference mainly comes from the calculation error of the volume. As a result, the shape of a microlens can be determined precisely by controlling the number of printed droplets. The fabricated MLA has an $F_{\#}$ ranges from 1.20 to 1.45, which means that a strong MLA (small $F_{\#}$) is acquired comparing to the traditional IJP method ($F_{\#}$>5). Moreover, the shape of the microlens can be fine-tuned using following parameters, such as the viscosity of the ink, the surface energy of both hydrophilic and hydrophobic regions, and the film-thickness of SAM. Most importantly, the solid content of lens materials is also a key parameter to determine the final morphology of the lens.[49]

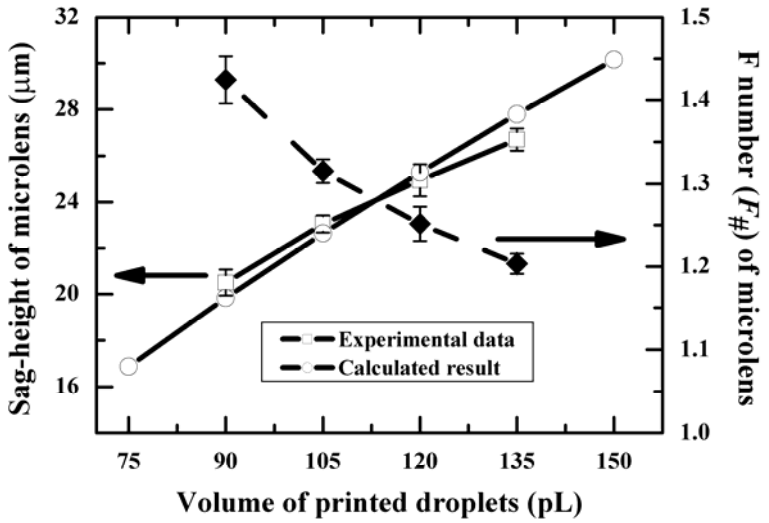

Figure 5.3 Sag-height and $f_{\#}$ of fabricated MLAs plotted against the function of the volume of printed droplets.

The surface of the substrate becomes hydrophobic due to the SAM and thereby reduces the adhesion of the lens material. As a result, a MLA with high fill-factors is achieved because the hydrophilic lens material is confined. Furthermore, the fill factor of the fabricated MLA is 65%, which is determined by the patterns of the SAM (FOTS). It reaches 75% if the circle pattern is replaced by a rectangular one and reaches 90% if the spacing is as small as 5μm. In addition, the size of the microlens can be changed by varying the size of the ink-jet head and the pattern of the PDMS stamp. In contrast to the traditional method, such as hot-embossing, which always faces the problem of shrinkage, the proposed microlens does not shrink due to its 100% NOA65 content. Furthermore, NOA65 is highly transparent and acts as an index-matching material to glass and other plastic substrates. Most of the optical loss, such as the internal reflection and wave-guiding effect, can thus be eliminated. Most importantly, the fabrication process of the MLA can be undertaken under normal room temperature; therefore, it is possible for it to be integrated into flexible devices in the future.

To enhance the light out-coupling efficiency of a PLED, the fabricated MLA was integrated on it using an index-matched material to reduce its optical loss. Only 20% of light generated in the PLED is observed (external mode), the others either emit out from the side-walls (wave-guided mode) or been adsorbed by materials. The MLA converts a portion of wave-guiding mode to the external node due to its geometric structure. As a result, the out-coupling efficiency of the PLED was enhanced 22±2% after incorporated with the MLA (diameter 100μm, sag-height 25μm, and spacing 10μm). To estimate the optical properties of the PLED, far-field luminance and was measured using a photometer, Minolta CS-100. The distance between the PLED and photometer is 1 meter. Figure 5.4a shows the viewing angle dependence normalized intensity of the PLED incorporated with a MLA comparing to that of a Lambertian surface and a bare PLED. We can see that the intensity of the PLED has a cosθ-dependence to its contact angle. The intensity of the PLED at large viewing angles is enhanced when a MLA is incorporated. To study the viewing angle dependence color-difference of the PLED, the color-coordinates were measured using a conoscope. Figure 5.4b shows the viewing angle dependence color-coordinates of the PLED with/without a MLA. We can see that the color-difference increases as the viewing angle increases. The color-difference (Δuv) of the PLED with/ without MLA at normal direction is 0.0022, which is smaller than the minimum perceptible color-difference value (0.0035) CIE UCS 1960. The difference is too small to be distinguished by human eyes. Moreover, the color-difference is reduced due to the integrated MLA because the light generated from the active layer can emit directly with less wave-guiding effect.

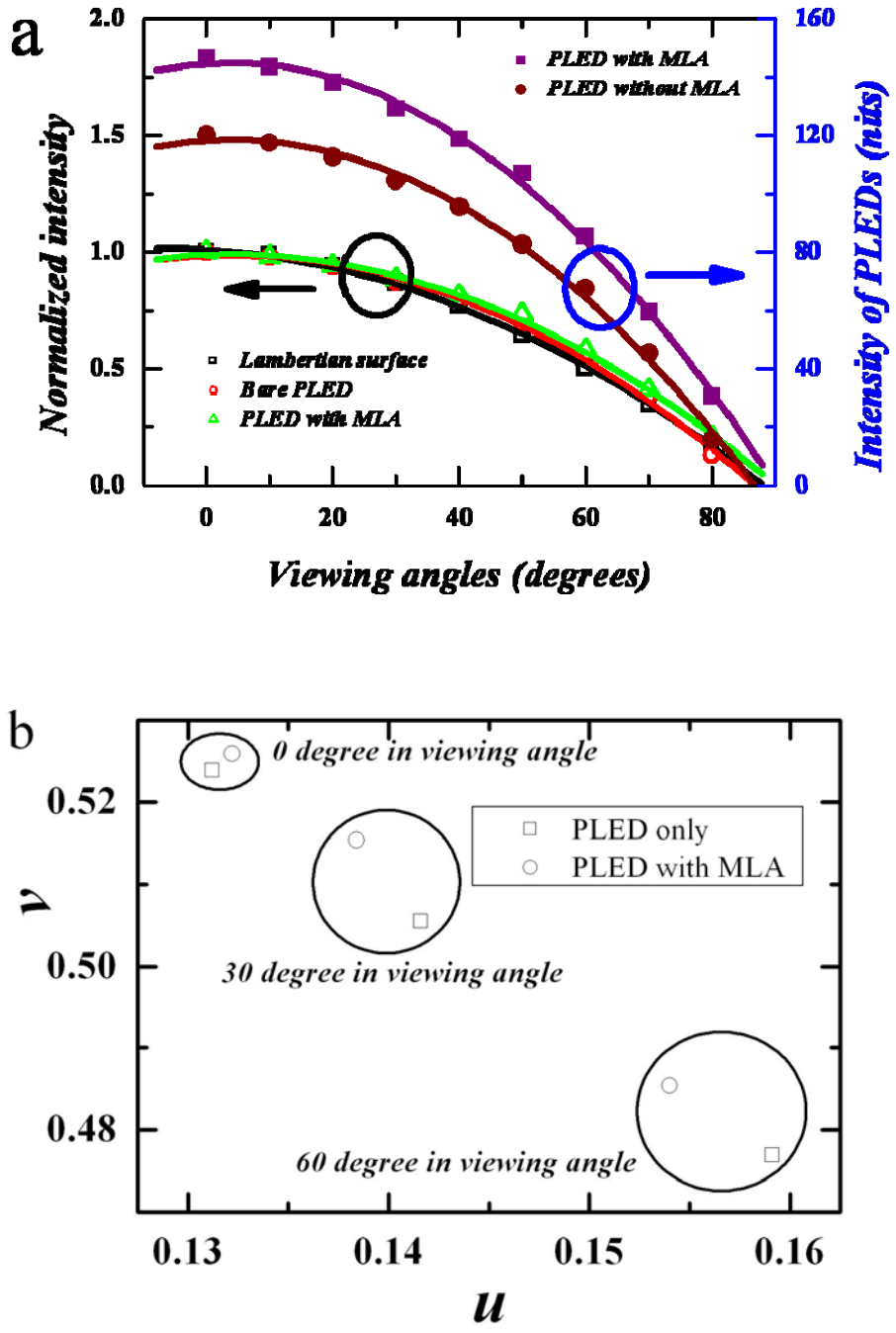

Figure 5.4 (a) The viewing angle dependence plotted against the normalized intensity of the PLED; (b) The viewing angle dependence color-coordinates of the PLED with and without an incorporated MLA.

5.4 Conclusion

A self-organized microlens array was fabricated using ink-jet printing on a pre-patterned substrate of self-assembled monolayer. The fabricated MLA has diameters ranges from 50 to 100μm, spacing from 5 to 15μm, and f number from 1.45 to 1.20 (100μm MLA). After the MLA integrated into a PLED, the out-coupling efficiency of the PLED was enhanced 22%. The emitted light-intensity of the PLED incorporated with a MLA was cosθ-dependence to its viewing angle θ and induced little color-difference. The proposed fabrication method is simpler comparing to traditionally photolithographic process. Moreover, the fabricated MLA has potential to be integrated into flexible devices because all process is accomplished at room temperature.

Chapter 6 Conjugated Polymer/ PCBM Bulk Hetero-junction Photovoltaic Devices under Outdoor Operating Conditions

6.1 Introduction

Organic photovoltaic (OPV) devices have become the focus of research due to their specific advantages such as their flexibility, portability, low fabrication cost, and suitability for large-area applications.[50, 51] Recently, organic solar cells, consisted of poly(3-hexylthiophene) (P3HT) and 6,6-phenyl C61-butyric acid methyl ester (PCBM) blend as the active layer, are the focus of attention due to their high power-conversion efficiency.[52, 53] Many groups have been involved extensively in this field and have focused on the following areas: light-absorption efficiency, the morphology of active layers, the mechanism of charge carriers' dissociation and transportation, and the power conversion efficiency of OPV devices. Most of the electro-optical characteristics of organic solar cells are measured under a well controlled environment in laboratories and follow the standard test conditions (STC): normal and unpolarized light, 1000 W/m^2 of irradiance, AM1.5G spectrum and 25°C of cell temperature. However, the outdoor environmental conditions are different from indoor such as the reflection of light, the variation of spectrum, the flow of wind, the intensity of light and the temperature of the devices. This variation in performance is very significant due to the fact that the irradiance of sun varies dramatically with time and weather. The operating temperature increases while solar energy is absorbed by these devices. Moreover, the temperature differs significantly depending on the longitude and season. In this study, the temperature and luminance effects on the P3HT/ PCBM OPV devices are demonstrated and their behaviors are analyzed. Most importantly, an optimum operating condition is found which enhances the power

conversion efficiency of OPV devices.

6.2 Results and discussion

Figure 6.1 shows the illumination dependence *J-V* characteristics of an OPV cell. Under short circuit conditions, the voltage between the cathode and anode is zero and the short circuit current density (J_{SC}) is proportional to the luminance (L) of the light source. The J_{SC} is composed of diffusion current (J_{diff}), which is produced by the carrier diffusion from the P3HT: PCBM interface, and a reverse drift current (J_{drift}), which is produced by the built-in potential of the device.[54] Under the flat band condition, the J_{drift} approaches to zero owing to the disappearance of the internal built-in electric field and only the J_{diff} exits due to the dissociation of excitons induced by solar irradiation. The flat band voltage (V_{FB}) equals the difference in work function between the cathode and anode. Under open circuit conditions, the J_{diff} is balanced off by a forward J_{drift}, which is induced by the forward bias voltage (V_F), to get a zero output current. The open circuit voltage (V_{OC}) is composed of V_{FB}, which comes from the difference in work function of the electrodes, and V_F, which provide an internal electric field to generate the J_{drift} in order to compensate the J_{diff}. From Figure 6.1, it can be seen that the J_{diff} increases as the illumination increases; however, a greater amount of J_{drift} is required to compensate the J_{diff} in the open circuit conditions. As a result, the *Voc* increases owing to the increase of the compensating voltage V_F, and its value is from 0.56 up to 0.69 *V* as the luminance of light source increases from 0.28 to 10.00 kW/m^2 in room temperature.

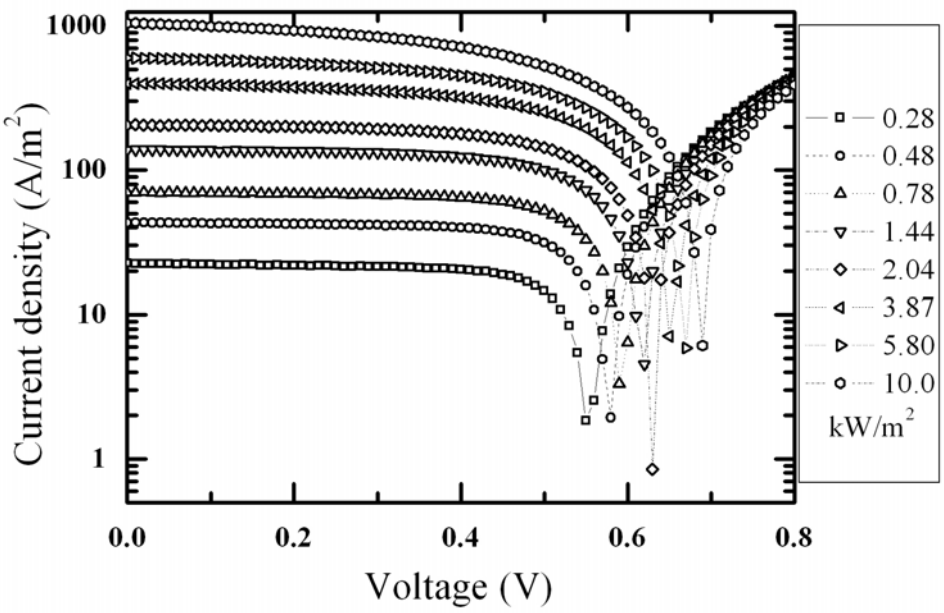

Figure 6.1 Current-voltage characteristics of a P3HT/ PCBM OPV cell under various illuminations.

In contrast, the V_{OC} decreases linearly with an increase in the temperature of device and varies depend on illumination levels, as shown in Figure 2(a). The measured temperature coefficient of V_{OC} ranges from -1.7 to -1.0 mV/K while the illumination varies from 0.28 to 10.00 kW/m^2. This decrease in V_{OC} across the temperature range is similar to the corresponding values of other conjugated polymer/ fullerene bulk hetero-junction OPV devices.[55, 56] The V_{OC} at $T= 0K$ can be extrapolated from the preliminarily experimental results and its value is 1.02 V, which is the upper limit value of the device and is independent on illumination. As a result, the V_{OC} is determined by either the illumination for its offset values or the temperature for its reduction rate ($d\,V_{OC}/d\,T$).

The current-voltage characteristic of OPV devices is similar to a photodiode and can be represented in the following formula:

$$I = I_s\left[\exp\left(\frac{qV}{\kappa T}\right)-1\right]-I_{ph},$$

where I_s is a reverse saturation current and I_{ph} is a reverse photocurrent with illumination. Then, the V_{OC} can be directly deduced from the formula with I=0:

$$V_{OC} = \frac{\kappa T}{q}\log\left(\frac{I_{ph}}{I_s}+1\right) \cong a - bT,$$

where $a = V_{OC}(T = 0K)$, and $b = -\frac{dV_{OC}}{dT}$ when $I_{ph} \rangle\rangle I_s$.

The simple model of a photodiode can be used in the conjugated polymer/ fullerene OPV devices due to their similar thin-film device structure and physical properties, such as the process of light absorption, excitons generation, carrier dissociation, and electron-hole collection. Most importantly, the linear decrease of the *Voc* with temperature variations is similar in behavior to that of an inorganic photodiode in the same conditions. The V_{OC} is directly related to the HOMO level of the donor ($HOMO_{donor}$) and the LUMO level of the acceptor ($LOMO_{acceptor}$) in the organic active layer. When the electrodes of OPV devices are ohmic contacts, the work functions of anode and cathode match the $HOMO_{donor}$ and the $LOMO_{acceptor}$, respectively. Furthermore, the Fermi levels of the anode and cathode are pinned to both the $HOMO_{donor}$ and the $LOMO_{acceptor}$ with the same contacts. Then, the *Voc* corresponds to the energy difference between the $HOMO_{donor}$ and the $LOMO_{acceptor}$. Moreover, it is similar to the differences in the work function of the electrodes. [57] In this study, P3HT ($HOMO_{donor}$ 4.9*eV*) and PCBM ($LOMO_{acceptor}$ 3.7*eV*) are used as the donor and acceptor materials of the active layer respectively, and their difference in work function is 1.2*eV*. Due to the band bending at the ohmic contact points, the *Voc* is reduced by 0.2 *V* for each contact and this difference has a lower limit of 0.8 *V*. As a result, the *Voc* at *T = 0* should be located between its lower limit of 0.8 *V* and its upper limit of 1.02 *V*.

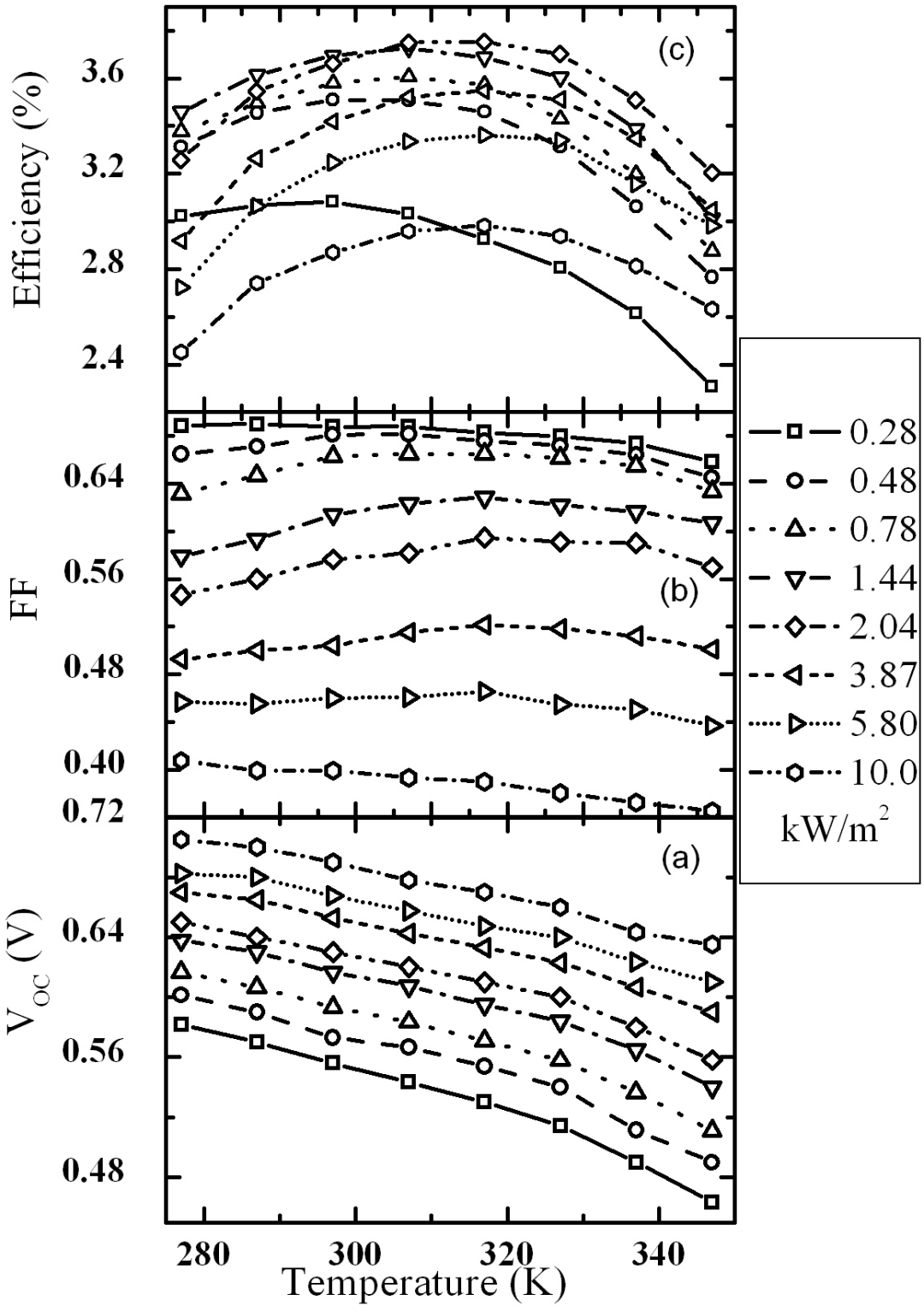

Figure 6.2 Illumination and temperature dependence of the (a) open circuit voltage, (b) fill factor, and (c) power conversion efficiency on an OPV cell.

Figure 6.2(b) shows the luminance and temperature dependent fill factor (*FF*) of the OPV devices. The *FF* was calculated using the following formula: $FF = \frac{V_m \times J_m}{V_{oc} \times J_{sc}}$, where the V_m and J_m are the voltage and current density of the maximum generated power, respectively. It can be seen that the *FF* increases slightly with an increase in temperature and then decreases gradually. The temperature of the highest *FF* increases with an increase in illumination. In contrast, the *FF* decreases gradually with an increase in temperature when the illumination is more than 10 Suns. It is obvious that the *FF* decreases dramatically with an increase in illumination because the V_{oc} and J_{sc} are proportional to the illumination, but the J_m decreases due to a lower carrier dissociation probability and a higher electron-hole recombination rate.

Figure 2(c) shows the luminance and temperature dependence power conversion efficiency (η) of the OPV devices. The η was calculated using the following formula: $\eta = \frac{FF \times V_{oc} \times J_{sc}}{L}$, where *L* represents the luminance of the light source. It can be seen that the η increases with an initial increase in illumination, up to the maximum value when the illumination is more than one sun, and then decreases gradually under high illumination conditions. The inter-related dependence of J_{SC} on *L* results in a constant ratio when the illumination level changes; however, the changes in V_{OC} and *FF*, which depend on illumination, are totally different. Therefore, when the J_{SC} and *L* values are removed because of their dependence on each other, the value of η is completely determined by the *FF* and V_{OC} values. As a result, the maximum value of η is 3.75% when the OPV cell is operated under 2 Suns near 320 K.

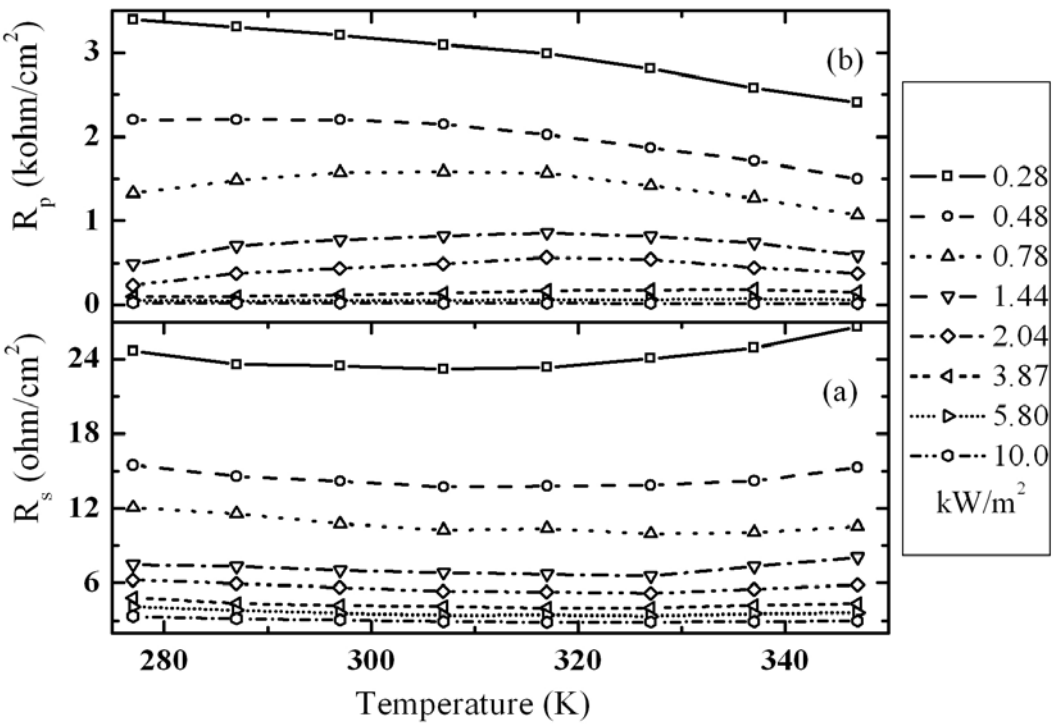

Figure 6.3 Illumination and temperature dependence of the (a) series, and (b) shunt resistances of an OPV cell.

Figures 6.3 shows the series resistance (r_s) and the shunt resistance (r_p) of the OPV devices under different temperatures and illuminations. The r_s and r_p are deduced from the *J-V* characteristics of the OPV devices under open circuit and short circuit conditions, respectively; where $r_s^{-1} = \left[\frac{dI}{dV}\right]_{I=0}$ and $r_p^{-1} = \left[\frac{dI}{dV}\right]_{V=0}$. It can be seen that the r_s decreases with an increase in illumination, results in more generated power, which corresponds to the increases of both J_{SC} and V_{OC} due to the lower levels of power consumption inside the OPV devices. However, the r_p also decreases due to the increase in illumination. The increase of the maximum available power, which is determined by J_m * V_m, is less than the increase of the area of the third quadrant of the graph which represents the *J-V* characteristics of the OPV devices. As a result, the *FF* of the OPV devices decreases with an increase of illumination. In an ideal case, the

generated power of the OPV devices is the maximum when r_s = 0 and $r_p \sim \infty$. From Figure 6.3, r_s is the minimum and r_p is the maximum during the temperature range from 310 to 320K, which is corresponding to the results of the highest power conversion efficiency.

Mobility is an important parameter used to determine the external quantum efficiency of OPV devices in the study of charge carrier transport under different operating temperature. Several methods have previously been used to calculate electron and hole mobility, such as the photocurrent measurement of the time of flight (TOF),[58] the *J-V* characteristics measurement of the field effect transistor (FET),[59] and the best-fit *J-V* curve using the space charge limit current (SCLC) model.[55] In this research, the SCLC method is used to determine mobility because the configuration of OPV devices, the film-thickness on the active layer, and the operating conditions are the same as those of actual devices. Hole and electron mobility can be determined from the *J-V* measurements of the hole-only and electron-only devices, respectively. To fabricate the hole-only device, molybdenum oxide (MoO_3, work function 5.3eV) and Al were thermally evaporated to form the top electrode in an indium tin oxide (ITO)/ PEDOT: PSS/ P3HT: PCBM structure. MoO_3 is a good hole injection material to suppress electron injections from the cathode due to a large difference between its work function and the lowest unoccupied molecular orbital (LUMO) of PCBM. In contrast, cesium carbonate (Cs_2CO_3, work function 2.9eV) was used as an efficient electron injection layer to replace PEDOT: PSS on the anode in order to make electron-only devices.

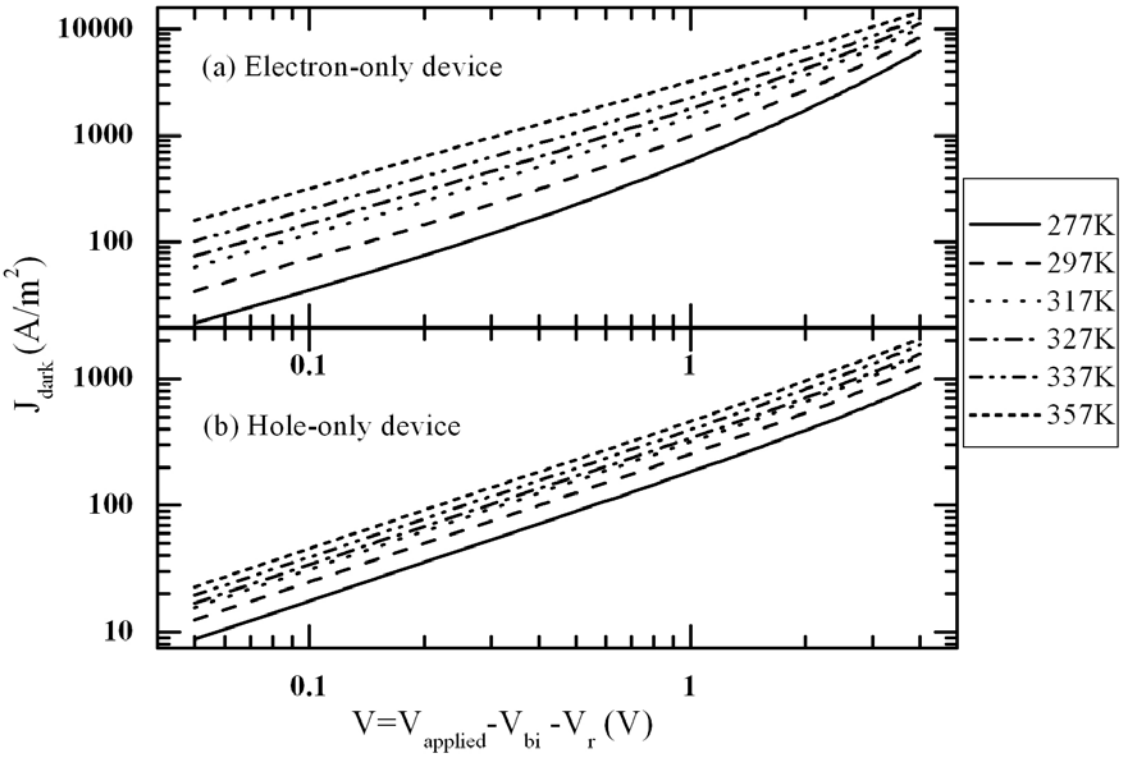

Figure 6.4 Double logarithm dark *J-V* characteristics for (a) hole-only and (b) electron-only devices operated under temperature ranges from 277 to 357K.

Figure 6.4 shows the double logarithm *J-V* characteristics without the existence of illumination for (a) hole-only and (b) electron-only devices which were operated under temperature range from 277 to 357K. In this model, the voltage is the result of the applied voltage minus both the built-in potential (V_{bi}), which comes from the work function difference of electrodes, and the voltage drop (V_r), which results from contact and series resistance. We can see that $J_{d\text{ark}}$ (current density in the absence of illumination) increases as the operating temperature increases, which induce a positive temperature coefficient. For example, the $J_{d\text{ark}}$ increases 2.5 and 5.5 times during operation at 1V bias under the temperature range from 277 to 357K for hole- and electron-only devices, respectively. The mobility of the hole- and electron-only devices can be calculated from Figure 6.4 using the best-fit *J-V* curve using the

following formula:

$$J_{dark} = \frac{9}{8}\varepsilon_0\varepsilon_r\mu\frac{V^2}{L^3}$$

where J_{dark} is the electron (or hole) current density; ε_0 the permittivity of the free space; ε_r the relative permittivity of the material; μ the mobility of the electrons (or holes); and L the thickness of the active layer. Figure 6.5 shows the calculated mobility of electrons and holes as a function of the operating temperature. We can see that the hole mobility increases from 7.8×10^{-8} to 1.8×10^{-7} m^2/Vs while the operating temperature increases from 277 to 357K. In contrast, the electron mobility is 1.3×10^{-6} m^2/Vs at 277K and increases gradually to its maximum value of 1.6×10^{-6} m^2/Vs at 337K; then, it decreases to 1.2×10^{-6} m^2/Vs at 357K. This result is comparable to the tendency of the power conversion efficiency of P3HT: PCBM blended OPV devices operated in the same temperature range. The transportation of the charge carriers becomes more efficient and the amount of photocurrent generated increases due to the increase in electron- and hole- mobility. As a result, more electric power is generated and the power conversion efficiency is the maxima when the operating temperature is about 320K. The results show that the electron- and hole-mobility have a relationship which is similar in that they both increase until the temperature reaches 337K. However, this relationship is not proportional because the rise in the former is more dramatic than the rise in the latter. Furthermore, after the specified temperature, the two are considerably different in performance: the former declines sharply while the latter continues to rise gradually.

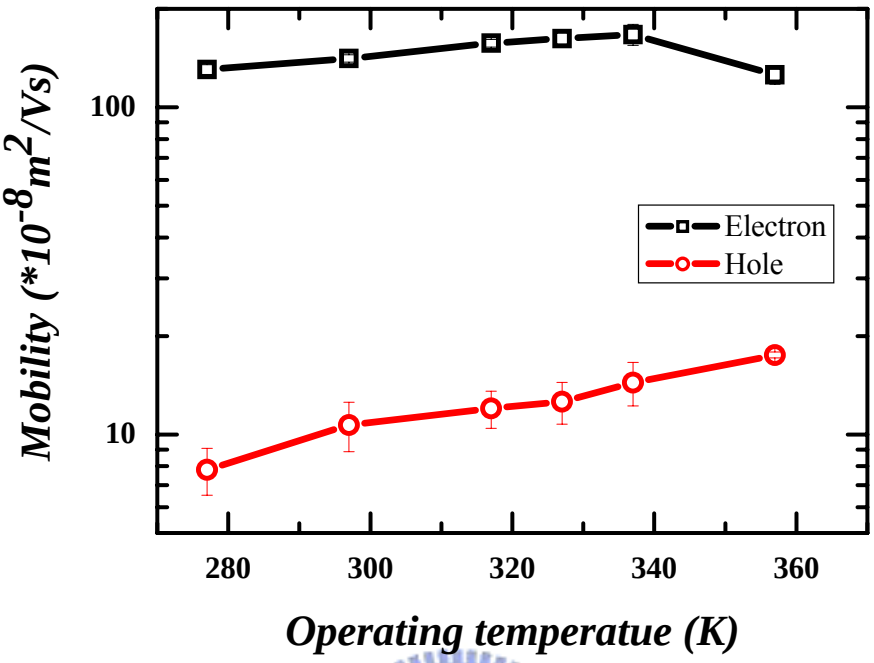

Figure 6.5 Electron- and hole- mobility of a P3HT/PCBM solar cell calculated from the dark *J-V* characteristics using the SCLC model.

In order to determine how the temperature influences the behavior of the OPV devices, P3HT was analyzed using a differential scanning calorimeter (DSC), as shown in Fig 6. The DSC diagram shows that the glass transfer temperature (Tg) of P3HT is about 100 ℃ and its melting temperature (Tm) is near 235 ℃. With respect to the DSC measurements, two sharp spikes can be observed at 307.5K and 326.8K, which are the melting points of the P3HT side-chains. From the above, it can be assumed that the enhancement of electron-mobility is due to the self-organization of the PCBM molecules during the temperature increase which improves the transportation efficiency of the electrons; however, ,the melting side-chains interrupt the continuity of the PCBM molecules and causes a decrease in electron-mobility.

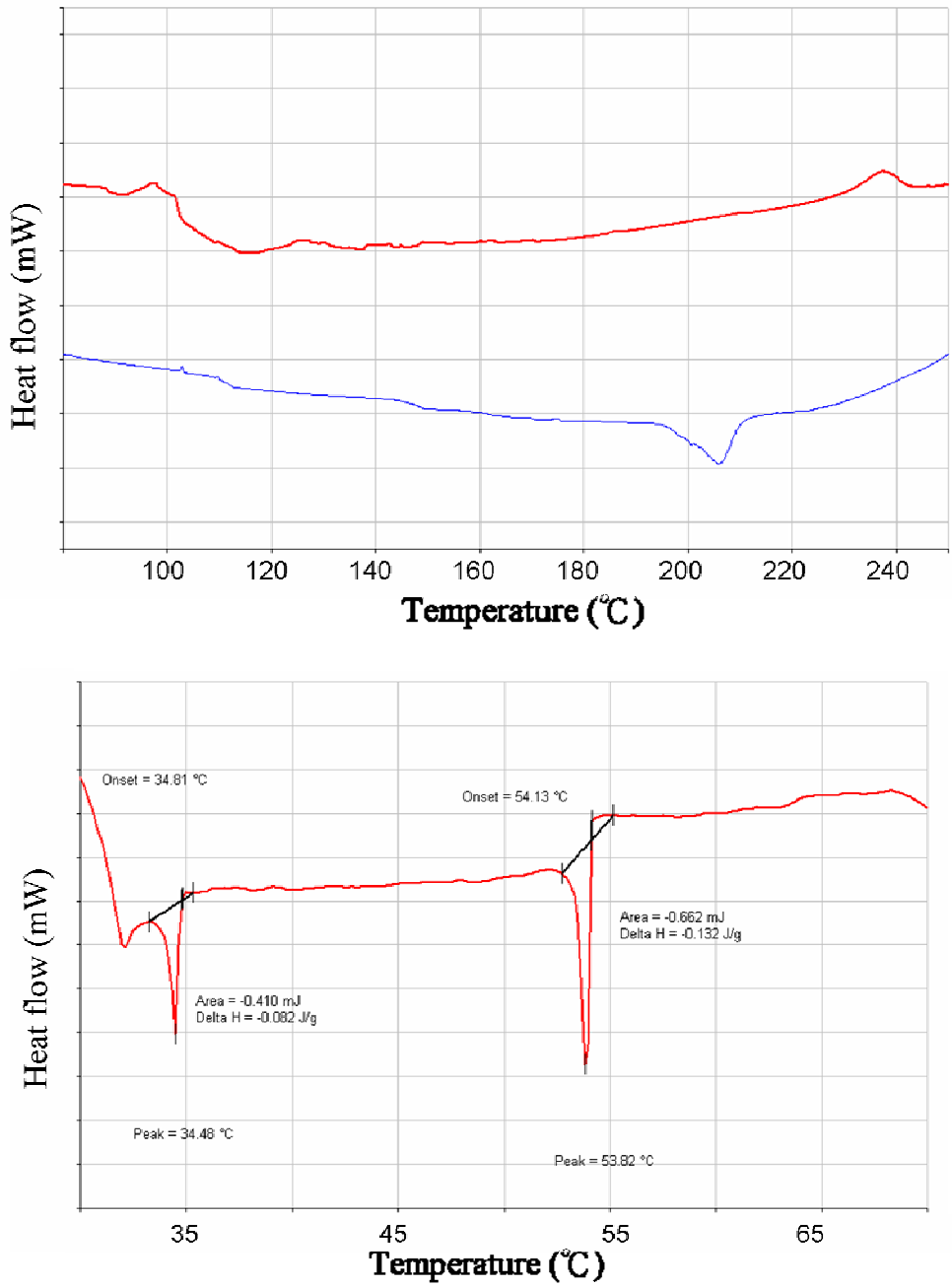

Figure 6.6 Heat-flow diagrams measured using a DSC in the temperature ranges of (a) 80-250, and (b) 30-70 ℃

To study the effect of illumination on the generation of photocurrent in the device, the *J-V* characteristics were measured in voltages ranging from 1 to -10V under illumination levels ranging from 1.06 to 7.74 kW/m^2. Figure 6.6 shows the dependence of the photocurrent (J_{ph}) on the level of illumination as it relates to the

effective applied voltage (V_{eff}). The current under illumination (J_{light}) minus the dark current (J_{d}ark) results in J_{ph}; i.e. $J_{ph} = J_{light} - J_{dark}$. V_{eff} is the result of V_0 minus the applied voltage (V), where V_0 is the voltage when J_{ph} = 0. We can see that J_{ph} is proportional to the V_{eff} when V_{eff} < 0.1 owing to the increase in drift current (J_{drift}) produced by the forward bias. As the V_{eff} increases, the J_{ph} increases gradually due to the result of diffusion current and reverse drift current. The J_{ph} becomes saturated at even higher voltages and is independent of the influence of both electric field and operational temperature. The maximum exciton generation rate (G_{max}) of polymer OPV devices can be calculated using the formula $J_{sat} = eG_{\max}L$ where J_{sat} is the saturated photocurrent and L (200nm) is the film-thickness on the active layer. In this study the G_{max} was increased form 2.91×10^{27} to $2.58\times10^{28}\,m^{-3}s^{-1}$ while the illumination was increased from 1.06 to 7.74 kW/m^2. As a result, the exciton generation rate is proportional to the light intensity (L).

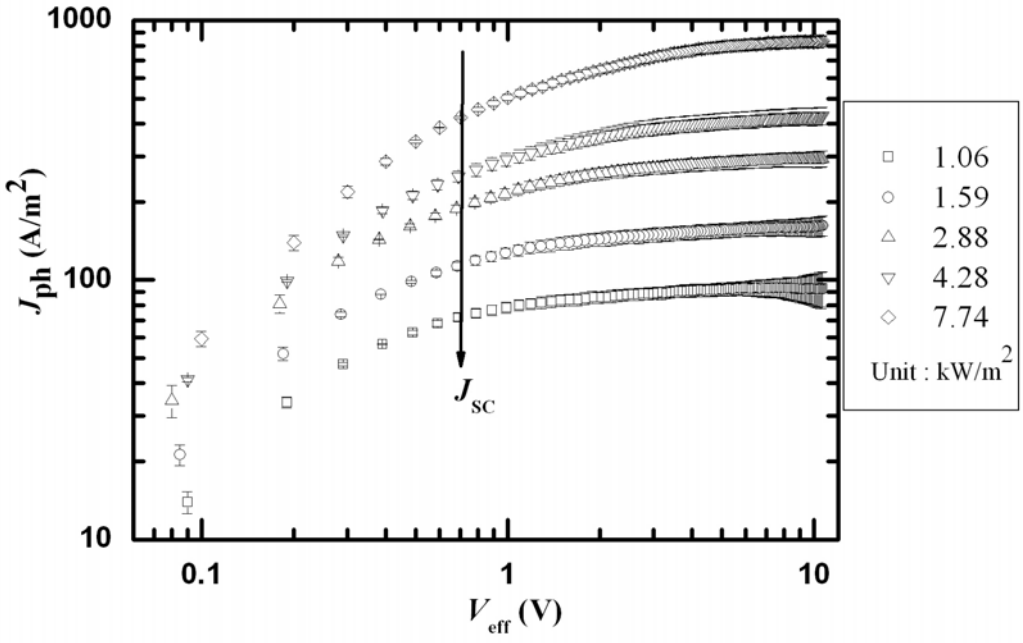

Figure 6.7 Illumination dependence of photocurrent (J_{PH}) as a function of effective applied voltage (V_{eff}).

Figure 6.8 shows the normalized photocurrent density under illumination as a function of the V_{eff}. When the value of J_{ph} / J_{sat} approaches 1 in the high V_{eff} region, it means that the generated excitons have completely become free carriers and the dissociation probability (P) is near 100%. We can see that P is as high as 0.77 in short circuit conditions under 1 Sun, which means that most excitons generated from the light exposure have become the photocurrent. The P decreases to 0.46 while the illumination increases from 1.06 to 7.74 kW/m^2 under the same conditions. Although more excitons are generated under high illumination, the value of P is limited by the recombination of the newly produced electron-hole pairs in the active layer instead of their separation or dissociation into free carriers. Similarly, the P decreases from 0.51 to 0.20 at the point of maximum generated power (V_{eff}= 0.3V) while the illumination increases from 1 to near 8 Suns. As a result, the FF and efficiency of the OPV devices decrease to the same extent as the Jm when the light exposure increases.

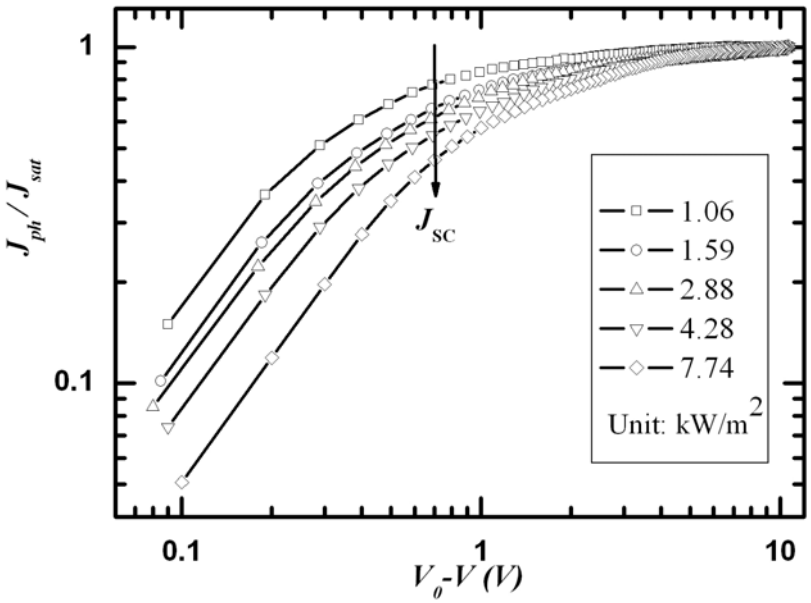

Figure 6.8 Normalized photocurrent densities under illumination as a function of the V_{eff}.

6.3 Enhanced power conversion efficiency of OPV devices using MLAs

From experimental results, the optimized operating condition of OPV devices is 320K under 2 Suns illumination, which leads the highest power conversion efficiency 3.75%. In order to acquire 2 Suns illumination, light condensing systems can be used to increase the power density of solar irradiation. Traditionally, a condensing mirror is used to reflect the solar irradiation on the surface of OPV devices and the power density is multiplied due to the concave mirror. However, the tilt angle of the mirror has to change all the time depending on the position of solar. In this dissertation, a novel method is proposed to increase the power density of solar irradiation using a microlens array (MLA). MLAs are assembled on the surface of OPV devices using a reflective index-matched material; therefore, the tracing of solar position is unnecessary. Moreover, the optical power is lost when the illumination is out of the active layer region of OPV devices. The MLA condenses solar irradiation to fit the area of active layer; as a result, the power efficiency of OPV devices is enhanced.

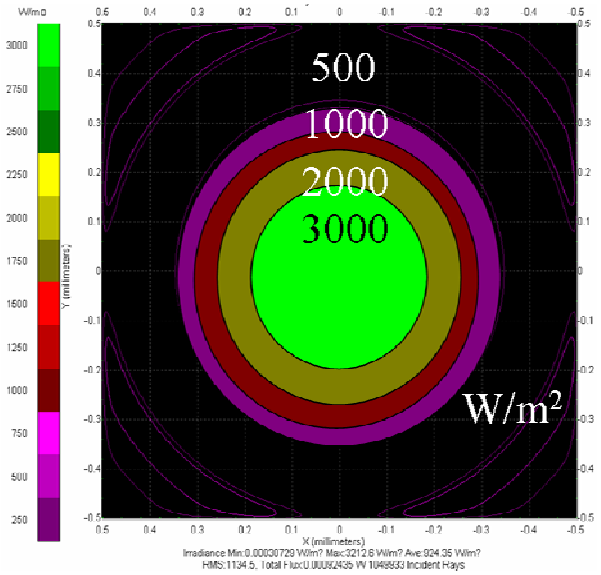

Figure 6.9 Illumination distribution of OPV devices incorporated with MLAs ($f_{\#}$=1) under 1 Sun.

Figure 6.9 shows the power distribution of solar irradiation (1 Sun) when OPV devices incorporated with MLAs ($f_{\#}$=1). It can be seen that the power distribution is circular symmetry and the power density increases to three fold due to the function of MLAs. Figure 6.10 shows the area-ratio dependent enhanced factor of solar illumination as a function of $f_{\#}$, which is simulated using TracePro. The area-ratio is the ratio of MLAs area to the active layer area and the enhanced factor is the enhancement of power density. It can be seen that the enhanced factor increases as the area-ratio increases and the $f_{\#}$ decreases. From the simulated results, a suitable area-ratio (> 2) and $f_{\#}$ (< 1.2) condition is determined as the gray box region which leads to a maximum power conversion efficiency of OPV devices.

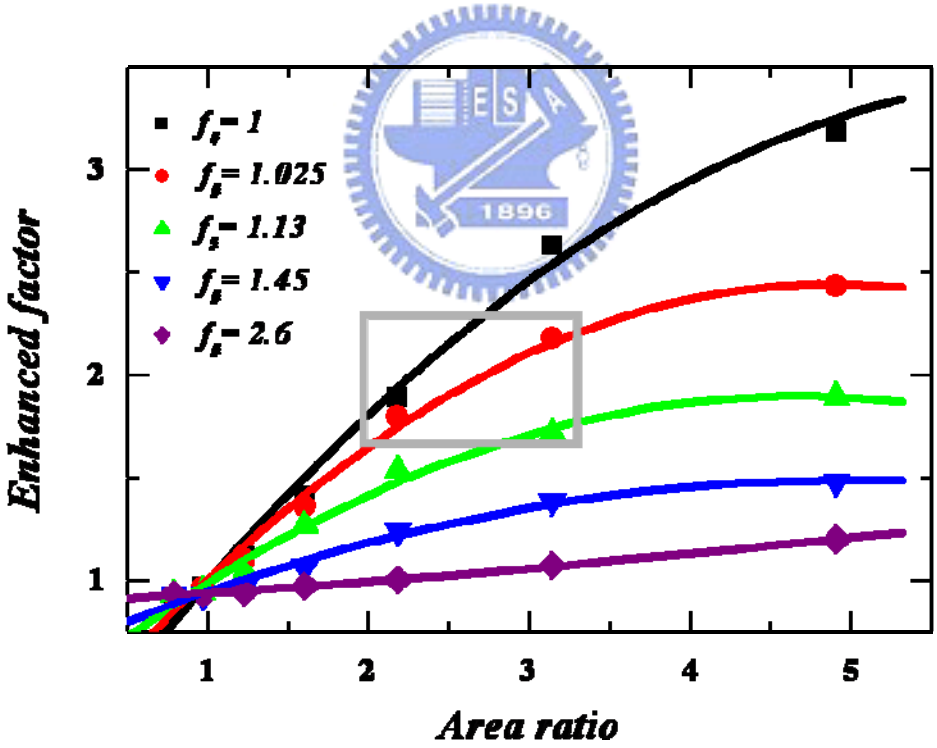

Figure 6.10 Area-ratio dependent enhanced factor of solar illumination as a function of $f_{\#}$. The gray box implies suitable parameters of area-ratio and $f_{\#}$ to fit the optimized operating conditions of OPV devices.

6.4 Conclusion

In conclusion, the performance of P3HT/PCBM bulk heterojunction OPV devices under different temperatures and illuminations has been demonstrated. Both the short circuit current and the open circuit voltage increase with an increase of illumination. Furthermore, the open circuit voltage decreases with an increase of temperature from – 1.0 to – 1.7 mV/K under the illumination level from 0.28 to 10.00 mW/cm^2. In contrast, the fill factor, series resistance, and shunt resistance decrease with an increase of illumination. Moreover, the power conversion efficiency, which is determined by the parameters of J_{SC}, V_{OC}, FF, and L, has the highest value when the illumination is near 2 Suns. The FF and η are enhanced within the temperature range from 310 to 320K due to the effectiveness of electrons-hole generation and charge carrier transportation. In this study, the optimal operating condition of the organic solar cell has been investigated and the power conversion efficiency has been found to be 3.75 %, which is suitable for the application of portable products.

Chapter 7 Summary and Conclusion

This dissertation includes three parts: the fabrication of a self-assembled microlens array (MLA), the enhancement of the light out-coupling efficiency of polymer light-emitting diodes (PLED) using a self-organized MLA, and the performance of organic photovoltaic (OPV) devices under outdoor operating conditions. The materials used in these devices are polymers; therefore, their physical properties (such as refractive index, viscosity, and surface energy) and fabrication processes (such as spin coating, ink-jet printing, and screen printing) are similar. As a result, the MLA can be integrated into PLEDs or OPV devices to enhance their performance. Moreover, these devices have the potential to be fabricated on flexible substrates due to their malleability and low fabrication temperature (< 200 ℃). The major difference between these devices is in the area of function; in short, the PLED is a light-emitting device, the OPV is a light-harvesting device, and the MLA is a light-deflection device.

The first part of the dissertation examines the fabrication of a self-assembled microlens array (MLA). The surface of a glass substrate is divided into hydrophilic and hydrophobic regions using UV-ozone treatment and micro-contact printing of the self-assembled monolayer (SAM), respectively. After the lens-material is deposited on the pre-patterned substrate, the hydrophilic lens-material is repelled by the hydrophobic SAM and self-organizes on the UV-ozone treated regions due to the difference in surface energy. Various lens-sizes and spacing are designed to fine-tune the fabrication parameters. The shape of the MLA is determined by the following parameters: viscosities of lens materials, surface energies of the substrate, fill-factors of the MLA, and the spin-rate of spin-coating process. To minimize the optical loss of

lens-substrate interface, an index-matching material (NOA65) is used to fabricate the MLA. NOA65 is an epoxy and can be solidified using UV-light curing. The morphology measured from the atomic force microscope shows that the fabricated MLAs have smooth surfaces with a surface roughness less than 1nm at the lens-center. The focused light-spots demonstrate a high level of uniformity of the MLA (deviation of focal length < 5%) and their spot-sizes are close to the theoretical diffraction-limit values. However, the drawbacks of the fabricated MLA are low curvature-radius and high f number ($f_{\#}$ >5), which limit its application. However, a strong MLA has been fabricated using ink-jet print instead of spin-coating.

The second part of this dissertation is to enhance the light out-coupling efficiency of PLED using the fabricated MLA. The out-coupling efficiency of PLED is low due to the occurrence of total internal reflection (TIR) at the air-substrate interface. To achieve the higher levels requirement of display and illumination applications, it is necessary to increase the driving power of a PLED; however, such an increase results in a decrease in the lifespan of a PLED. To extend the lifespan of a PLED, its external power conversion efficiency has to be improved. One effective approach is the enhancement of the light out-coupling efficiency of the PLED using a MLA. The light out-coupling efficiency of the PLED incorporated with an MLA is determined by factors such as refractive index and film-thickness of individual materials, and shape and fill-factor of the MLA, etc. In an ideal situation, the enhanced factor is the maxima when the PLED is located at the center of a much larger hemisphere microlens (tenfold larger in size). As a result, the PLED can be viewed as a point-light-source and light generated in the PLED can emit directly without refraction. However, a large lens is too heavy and voluminous to be applied to optical systems such as displays or illumination systems. Therefore, microlenses matched to individual pixels in a PLED is the most common approach in an optical

image system. However, it is difficult to align the MLA to an optical device without causing optical loss. In this dissertation, a self-organized MLA is integrated into a PLED to enhance its light out-coupling efficiency. The enhanced factor increases as the sag-height and fill factor of the MLA increase. Moreover, the viewing angle and color difference of the PLED are improved due to the change of surface structure. In addition, the two devices have been fabricated individually and then assembled using an index-matched material. The advantage of this process of fabrication is that the two devices will not interfere with each other and as a result their production is less complicated.

The final part of this dissertation reveals the performance of organic photovoltaic (OPV) devices under outdoor operating conditions. The characteristics of OPV devices are usually measured indoors under standard test conditions (STC) in which a solar simulator is used as a light source with an illumination of 1 kW/m^2 AM 1.5 G at 25℃. However, an outdoor-operated OPV has to face variation in luminance and temperature with changes in time and place. Therefore, it is very useful to discuss the influence of luminance (L) and temperature (T) on the outdoor performance of OPV devices. From the experiments conducted in this study, the short circuit current (Jsc) increases as the luminance level increases because more excitons are generated and these induce a larger diffusion current. In open circuit conditions, the output current is zero and the diffusion current is negated by a reverse drift current, which is induced by the built-in potential of the device. As a result, the open circuit voltage (Voc) also increases with an increase in luminance. In contrast, the fill factor (FF) decreases as the luminance level increases because the recombination rate of the charge-carriers also increases. The power conversion efficiency of the OPV device (η) is defined as the ratio of the generated carriers to the incident photons and is determined using Jsc, Voc, FF, and L. It can be seen that the highest η level is located at the luminance level

of nearly 2 Suns. The Voc decreases as the operating temperature increases with a temperature coefficient ranging from -1.7 to -1.0 mV/K while the illumination varies from 0.28 to 10.00 kW/m^2. In contrast, the Jsc, FF and η achieve their maximum when the temperature reaches 317K. The mobility of the electron-only and hole-only devices is calculated using a space charge limited current (SCLC) model. The results show that the electron- and hole-mobility have a relationship which is similar in that they both increase until the temperature reaches 337K. However, this relationship is not proportional because the rise in the former is more dramatic than the rise in the latter. Furthermore, after the specified temperature, the two are considerably different in performance: the former declines sharply while the latter continues to rise gradually. With respect to the DSC measurements, two sharp spikes can be observed at 307.5K and 326.8K, which are the melting points of the P3HT side-chains. From the above, it can be assumed that the enhancement of electron-mobility is due to the self-organization of the PCBM molecules during the temperature increase which improves the transportation efficiency of the electrons; however, ,the melting side-chains interrupt the continuity of the PCBM molecules and causes a decrease in electron-mobility.

Reference

[1] R. McNeill, D. E. Weiss, J. H. Wardlaw, and R. Siudak, "Electronic Conduction In Polymers.1. Chemical Structure Of Polypyrrole," Australian Journal Of Chemistry, 16, pp. 1056-&, 1963.

[2] B. A. Bolto and D. E. Weiss, "Electronic Conduction In Polymers.2. Electrochemical Reduction Of Polypyrrole At Controlled Potential," Australian Journal Of Chemistry, 16, pp. 1076-&, 1963.

[3] B. A. Bolto, R. McNeill, and D. E. Weiss, "Electronic Conduction In Polymers.3. Electronic Properties Of Polypyrrole," Australian Journal Of Chemistry, 16, pp. 1090-&, 1963.

[4] J. G. Lee, Y. G. Seol, and N. E. Lee, "Polymer thin film transistor with electroplated source and drain electrodes on a flexible substrate," Thin Solid Films, 515, pp. 805-809, 2006.

[5] G. H. Kim, S. M. Yoon, C. A. Kim, K. H. Baek, I. K. You, S. Y. Kang, S. D. Ahn, and K. S. Suh, "Plastic-based organic thin-film transistors with thermally cured polymeric gate dielectrics," Journal Of The Korean Physical Society, 49, pp. 1239-1242, 2006.

[6] Y. Shao, G. C. Bazan, and A. J. Heeger, "Long-lifetime polymer light-emitting electrochemical cells," Advanced Materials, 19, pp. 365-+, 2007.

[7] S. A. Haque, S. Koops, N. Tokmoldin, J. R. Durrant, J. S. Huang, D. D. C. Bradley, and E. Palomares, "A multilayered polymer light-emitting diode using a nanocrystalline metal-oxide film as a charge-injection electrode," Advanced Materials, 19, pp. 683-+, 2007.

[8] C. M. Yang, C. H. Wu, H. H. Liao, K. Y. Lai, H. P. Cheng, S. F. Horng, H. F. Meng, and J. T. Shy, "Enhanced photovoltaic response of organic solar cell by singlet-to-triplet exciton conversion," Appl. Phys. Lett., 90, 2007.

[9] S. Gunes, H. Neugebauer, and N. S. Sariciftci, "Conjugated polymer-based organic solar cells," Chemical Reviews, 107, pp. 1324-1338, 2007.

[10] S. K. Lee, K. C. Lee, and S. S. Lee, "A simple method for microlens fabrication by the modified LIGA process," J. Micromech. Microeng., 12, pp. 334-340, 2002.

[11] A. Y. Smuk and N. M. Lawandy, "Direct laser fabrication of dense microlens arrays in semiconductor-doped glass," J. Appl. Phys., 87, pp. 4026-4030, 2000.

[12] S. Mihailov and S. Lazare, "Fabrication Of Refractive Microlens Arrays By Excimer-Laser Ablation Of Amorphous Teflon," Appl. Optics, 32, pp. 6211-6218, 1993.

[13] A. Bernanose and P. Vouaux, "*Electroluminescence Organique - Etude Du Mode Demission," Journal De Chimie Physique Et De Physico-Chimie Biologique, 50, pp. 261-&, 1953.

[14] A. Bernanose, M. Comte, and P. Vouaux, "*Sur Un Nouveau Mode Demission Lumineuse Chez Certains Composes Organiques," Journal De Chimie Physique Et De Physico-Chimie Biologique, 50, pp. 64-68, 1953.

[15] C. W. Tang and S. A. Vanslyke, "Organic Electroluminescent Diodes," Appl. Phys. Lett., 51, pp. 913-915, 1987.

[16] M. H. Lu and J. C. Sturm, "Optimization of external coupling and light emission in organic light-emitting devices: modeling and experiment," J. Appl. Phys., 91, pp. 595-604, 2002.

[17] M. H. Lu and J. C. Sturm, "External coupling efficiency in planar organic light-emitting devices," Appl. Phys. Lett., 78, pp. 1927-1929, 2001.

[18] S. Moller and S. R. Forrest, "Improved light out-coupling in organic light emitting diodes employing ordered microlens arrays," J. Appl. Phys., 91, pp.

3324-3327, 2002.

[19] H. Hoppe and N. S. Sariciftci, "Organic solar cells: An overview," J. Mater. Res., 19, pp. 1924-1945, 2004.

[20] Q. M. Zhou, Q. Hou, L. P. Zheng, X. Y. Deng, G. Yu, and Y. Cao, "Fluorene-based low band-gap copolymers for high performance photovoltaic devices," Appl. Phys. Lett., 84, pp. 1653-1655, 2004.

[21] S. E. Shaheen, D. Vangeneugden, R. Kiebooms, D. Vanderzande, T. Fromherz, F. Padinger, C. J. Brabec, and N. S. Sariciftci, "Low band-gap polymeric photovoltaic devices," Synth. Met., 121, pp. 1583-1584, 2001.

[22] K. Hamanaka and H. Koshi, "An artificial compound eye using a microlens array and its application to scale-invariant processing," Opt. Rev., 3, pp. 264-268, 1996.

[23] N. Nordman and O. Nordman, "Optical properties of two photoresists designed for charge-coupled device microlenses," Opt. Eng., 40, pp. 2572-2576, 2001.

[24] R. Danzebrink and M. A. Aegerter, "Deposition of micropatterned coating using an ink-jet technique," Thin Solid Films, 351, pp. 115-118, 1999.

[25] D. L. Macfarlane, V. Narayan, J. A. Tatum, W. R. Cox, T. Chen, and D. J. Hayes, "Microjet Fabrication Of Microlens Arrays," IEEE Photonics Technol. Lett., 6, pp. 1112-1114, 1994.

[26] J. Sung, H. Hockel, J. Brown, and E. G. Johnson, "Refractive micro-optics fabrication with a 1-D binary phase grating mask applicable to MOEMS processing," J. Microlithogr. Microfabr. Microsyst., 4, 2005.

[27] C. W. Tang, "2-Layer Organic Photovoltaic Cell," Appl. Phys. Lett., 48, pp. 183-185, 1986.

[28] S. E. Shaheen, C. J. Brabec, N. S. Sariciftci, F. Padinger, T. Fromherz, and J. C.

Hummelen, "2.5% efficient organic plastic solar cells," Appl. Phys. Lett., 78, pp. 841-843, 2001.

[29] F. Padinger, R. S. Rittberger, and N. S. Sariciftci, "Effects of postproduction treatment on plastic solar cells," Adv. Funct. Mater., 13, pp. 85-88, 2003.

[30] C. J. Ko, Y. K. Lin, F. C. Chen, and C. W. Chu, "Modified buffer layers for polymer photovoltaic devices," Appl. Phys. Lett., 90, 2007.

[31] E. Kim and G. M. Whitesides, "Use Of Minimal Free-Energy And Self-Assembly To Form Shapes," Chem. Mat., 7, pp. 1257-1264, 1995.

[32] H. A. Biebuyck and G. M. Whitesides, "Self-Organization Of Organic Liquids On Patterned Self-Assembled Monolayers Of Alkanethiolates On Gold," Langmuir, 10, pp. 2790-2793, 1994.

[33] D. M. Hartmann, O. Kibar, and S. C. Esener, "Optimization and theoretical modeling of polymer microlens arrays fabricated with the hydrophobic effect," Appl. Optics, 40, pp. 2736-2746, 2001.

[34] D. M. Hartmann, O. Kibar, and S. C. Esener, "Characterization of a polymer microlens fabricated by use of the hydrophobic effect," Opt. Lett., 25, pp. 975-977, 2000.

[35] M. Keil, M. Beck, T. G. I. Ling, M. Graczyk, L. Montelius, and B. Heidari, "Development and characterization of silane antisticking layers on nickel-based stamps designed for nanoimprint lithography," J. Vac. Sci. Technol. B, 23, pp. 575-584, 2005.

[36] J. K. Chen, F. H. Ko, K. F. Hsieh, C. T. Chou, and F. C. Chang, "Effect of fluoroalkyl substituents on the reactions of alkylchlorosilanes with mold surfaces for nanoimprint lithography," J. Vac. Sci. Technol. B, 22, pp. 3233-3241, 2004.

[37] T. Bailey, B. J. Choi, M. Colburn, M. Meissl, S. Shaya, J. G. Ekerdt, S. V.

Sreenivasan, and C. G. Willson, "Step and flash imprint lithography: Template surface treatment and defect analysis," J. Vac. Sci. Technol. B, 18, pp. 3572-3577, 2000.

[38] C. D. Muller, A. Falcou, N. Reckefuss, M. Rojahn, V. Wiederhirn, P. Rudati, H. Frohne, O. Nuyken, H. Becker, and K. Meerholz, "Multi-colour organic light-emitting displays by solution processing," Nature, 421, pp. 829-833, 2003.

[39] Z. L. Shen, P. E. Burrows, V. Bulovic, S. R. Forrest, and M. E. Thompson, "Three-color, tunable, organic light-emitting devices," Science, 276, pp. 2009-2011, 1997.

[40] P. K. H. Ho, D. S. Thomas, R. H. Friend, and N. Tessler, "All-polymer optoelectronic devices," Science, 285, pp. 233-236, 1999.

[41] W. K. Huang, C. J. Ko, and F. C. Chen, "Organic selective-area patterning method for microlens array fabrication," Microelectron. Eng., 83, pp. 1333-1335, 2006.

[42] F. C. Chen, W. K. Huang, and C. J. Ko, "Self-organization of microlens arrays caused by the spin-coating-assisted hydrophobic effect," IEEE Photonics Technol. Lett., 18, pp. 2454-2456, 2006.

[43] J. L. Wilbur, A. Kumar, H. A. Biebuyck, E. Kim, and G. M. Whitesides, "Microcontact printing of self-assembled monolayers: Applications in microfabrication," Nanotechnology, 7, pp. 452-457, 1996.

[44] N. S. Ong, Y. H. Koh, and Y. Q. Fu, "Microlens array produced using hot embossing process," Microelectron. Eng., 60, pp. 365-379, 2002.

[45] T. N. Oder, J. Shakya, J. Y. Lin, and H. X. Jiang, "Nitride microlens arrays for blue and ultraviolet wavelength applications," Appl. Phys. Lett., 82, pp. 3692-3694, 2003.

[46] S. D. Moon, N. Lee, and S. Kang, "Fabrication of a microlens array using micro-compression molding with an electroformed mold insert," J. Micromech. Microeng., 13, pp. 98-103, 2003.

[47] G. Kopitkovas, T. Lippert, C. David, S. Canulescu, A. Wokaun, and J. Gobrecht, "Fabrication of beam homogenizers in quartz by laser micromachining," J. Photochem. Photobiol. A-Chem., 166, pp. 135-140, 2004.

[48] S. Biehl, R. Danzebrink, P. Oliveira, and M. A. Aegerter, "Refractive microlens fabrication by ink-jet process," J. Sol-Gel Sci. Technol., 13, pp. 177-182, 1998.

[49] J. Z. Wang, Z. H. Zheng, H. W. Li, W. T. S. Huck, and H. Sirringhaus, "Dewetting of conducting polymer inkjet droplets on patterned surfaces," Nat. Mater., 3, pp. 171-176, 2004.

[50] M. Keil, M. Beck, G. Frennesson, E. Theander, E. Bolmsjo, L. Montelius, and B. Heidari, "Process development and characterization of antisticking layers on nickel-based stamps designed for nanoimprint lithography," J. Vac. Sci. Technol. B, 22, pp. 3283-3287, 2004.

[51] C. J. Brabec, "Organic photovoltaics: technology and market," Sol. Energy Mater. Sol. Cells, 83, pp. 273-292, 2004.

[52] W. L. Ma, C. Y. Yang, X. Gong, K. Lee, and A. J. Heeger, "Thermally stable, efficient polymer solar cells with nanoscale control of the interpenetrating network morphology," Adv. Funct. Mater., 15, pp. 1617-1622, 2005.

[53] G. Li, V. Shrotriya, J. S. Huang, Y. Yao, T. Moriarty, K. Emery, and Y. Yang, "High-efficiency solution processable polymer photovoltaic cells by self-organization of polymer blends," Nat. Mater., 4, pp. 864-868, 2005.

[54] A. Moliton and J. M. Nunzi, "How to model the behaviour of organic photovoltaic cells," Polymer International, 55, pp. 583-600, 2006.

[55] D. Chirvase, Z. Chiguvare, M. Knipper, J. Parisi, V. Dyakonov, and J. C. Hummelen, "Temperature dependent characteristics of poly(3 hexylthiophene)-fullerene based heterojunction organic solar cells," J. Appl. Phys., 93, pp. 3376-3383, 2003.

[56] E. A. Katz, D. Faiman, S. M. Tuladhar, J. M. Kroon, M. M. Wienk, T. Fromherz, F. Padinger, C. J. Brabec, and N. S. Sariciftci, "Temperature dependence for the photovoltaic device parameters of polymer-fullerene solar cells under operating conditions," J. Appl. Phys., 90, pp. 5343-5350, 2001.

[57] V. D. Mihailetchi, P. W. M. Blom, J. C. Hummelen, and M. T. Rispens, "Cathode dependence of the open-circuit voltage of polymer: fullerene bulk heterojunction solar cells," J. Appl. Phys., 94, pp. 6849-6854, 2003.

[58] S. M. Tuladhar, D. Poplavskyy, S. A. Choulis, J. R. Durrant, D. D. C. Bradley, and J. Nelson, "Ambipolar charge transport in films of methanofullerene and poly(phenylenevinylene)/methanofullerene blends," Adv. Funct. Mater., 15, pp. 1171-1182, 2005.

[59] G. M. Wang, J. Swensen, D. Moses, and A. J. Heeger, "Increased mobility from regioregular poly(3-hexylthiophene) field-effect transistors," J. Appl. Phys., 93, pp. 6137-6141, 2003.